

BARIATRIC SURGERY-INDUCED CHANGES IN GUT MICROBIOTA ALTER
HOST GLUCOSE METABOLISM

BARIATRIC SURGERY ALTERS THE GUT MICROBIOTA AND BLOOD
GLUCOSE IN MICE

by Yuk Kwan Cassandra Chen, BSc.

A Thesis Submitted to the School of Graduate studies in Partial Fulfilment of the
Requirements for the Degree of Master of Science

McMaster University © Copyright by Yuk Kwan Cassandra Chen, August 2020

MSc. Thesis | Y Chen, McMaster University (Biochemistry)

McMaster University MASTER OF SCIENCE (2020) Hamilton, Ontario

(Biochemistry)

TITLE: Bariatric surgery alters the gut microbiota and blood glucose in mice

AUTHOR: Yuk Kwan Cassandra Chen, BSc (McMaster University)

SUPERVISOR: Dr. Jonathan D. Schertzer

NUMBER OF PAGES: xvi, 102

Lay Abstract

Type 2 diabetes is a chronic disease that involves high blood sugar (i.e. glucose), which can damage many parts of the body leading to serious complications.

Diabetes is a growing global problem and is the seventh leading cause of death.

Obesity is one of the largest factors leading to type 2 diabetes. Bariatric surgery reduces obesity and is to date the most effective method to lower blood glucose

and reverse type 2 diabetes. Bariatric surgery alters gut anatomy and the types

of bacteria that inhabit the gut. Gut bacteria can change obesity and blood

glucose levels, but it was not known if the bacterial community present after

bariatric surgery was a factor that is sufficient to lower blood glucose. We found

that transferring gut bacteria from humans after bariatric surgery into mice lowers

the blood glucose and alters the gut barrier structure where food is absorbed. It is

not yet clear how this happens, but these findings show that a change in gut

microbes is a standalone factor that can alter host blood glucose. Finding the

glucose lowering factor in bacteria may be a new treatment to combat type 2

diabetes.

Abstract

The prevalence of obesity is increasing globally. Obesity is characterized by increased fat mass and is a risk factor for type 2 diabetes (T2D). Obesity is associated with hyperglycaemia, hyperinsulinemia, insulin resistance and chronic inflammation. Currently, the most effective and durable treatment for obesity and its comorbidities is bariatric surgery. Bariatric surgery changes food intake, energy balance and the composition of gut microbiota. Bariatric surgery can lower blood glucose and put T2D into remission. It was unknown if bariatric surgery-induced changes in the gut microbiota was an independent yet sufficient factor to lower blood glucose. Fecal microbiota transplantation (FMT) was performed on conventional (specific-pathogen-free, SPF) and germ-free (GF) mice using fecal material obtained from patients before surgery and 12 months after bariatric surgery. We tested FMT into mice from the same patients before and after vertical sleeve gastrectomy (VSL) and biliopancreatic diversion with duodenal switch (BPD/DS). FMT did not alter body weight, fat mass, glucose tolerance or glucose transporter mRNA expression in all intestine segments in SPF mice. FMT lowered blood glucose during an oral glucose load in GF mice receiving bacteria after VSL and BPD/DS bariatric surgery. Post-BPD/DS surgery FMT decreased *Glut1* transcript level in the ileum and increased *Glut1* transcript level in the TA muscle of GF mice, but did not change GLUT1 protein levels. Post-BPD/DS surgery FMT also decreased goblet cell count, villus height and crypt depth in the ileum of GF mice. We conclude that changes in the gut

microbiota caused by bariatric surgery is a standalone factor that can lower blood glucose and alter gut morphology.

ACKNOWLEDGEMENTS

I would like to thank and acknowledge the numerous individuals who have helped and contributed to this project. The successful completion of my thesis would not have been possible without the support of these many people. My most sincere thanks goes to my supervisor, Dr. Jonathan Schertzer, without whom this research project would not have been possible. Thank you, Jon, for warmly welcoming me to your lab and making every effort to help me become a better scientist. Thank you for your amazing mentorship, encouragement and guidance throughout the two years. Your passion has greatly influenced me.

A special thank you to Dr. Fernando Forato Anê for your wisdom and constantly sharing your wealth of experience and knowledge in lab techniques. Thank you to Dr. Nicole Barra for helping me with my experiments and analyses, and for your continuous encouragement. I would also like to acknowledge all my fellow lab mates in the Schertzer lab: Dr. Kevin Foley, Dr. Brittany Duggan, Dr. Joe Cavallari, Dr. Brandyn Henriksbo, Dr. Trevor Lau and Michael Huang. I truly enjoyed coming to the lab every day to work with all of you. I wish you all the best in your academic pursuits.

Thank you to Christian Bellissimo for teaching me the microscopy skills that I needed to complete my histology analyses. Thank you to Dr. Deborah Sloboda for kindly allowing me to use your lab equipment.

Thank you to my supervisory committee members, Dr. Geoff Werstuck and Dr. Deborah Sloboda, for their invaluable guidance throughout my project.

Thank you to Mathilda Chow for your support and good sense of humour throughout my university life.

Finally, I would like to deeply thank my family and friends for their love, support and encouragement throughout my graduate studies.

TABLE OF CONTENTS

1.0 INTRODUCTION	1
1.1 Obesity and type 2 diabetes	1
1.1.1 Mechanisms underlying insulin resistance, type 2 diabetes and obesity	2
1.1.2 Prediabetes and glucose metabolism	5
1.2 Bariatric surgeries	10
1.2.1 Types of bariatric surgery	11
1.2.2 Impact of bariatric surgery on obesity	12
1.2.3 Mechanisms of bariatric surgery on type 2 diabetes remission	13
1.3 The intestinal microbiota	15
1.3.1 Obesity, bariatric surgery and gut microbiota	15
1.3.2 Effects of gut microbiota on blood glucose	19
2.0 RATIONALE, HYPOTHESES AND RESEARCH AIMS	22
2.1 Rationale	22
2.2 Hypothesis	22
2.3 Research aims	23
3.0 EXPERIMENTAL METHODOLOGY	24
3.1 Reagents and antibodies	24
3.2 Animal care and tissue collection	25
3.3 Serum analyses	28
3.4 Gene expression analysis	28
3.4.1 RNA extraction	28
3.4.2 cDNA synthesis	29
3.4.3 RT-PCR Reactions	30
3.5 Protein Analysis	31
3.5.1 Protein Extraction from tissues	31
3.5.2 Total Protein Measurements	31
3.5.3 Immunoblotting	32
3.6 Histology	33
3.6.1 Hematoxylin and Eosin Staining	33
3.6.2 Image analyses	33
3.7 Statistical analyses	34

4.0 RESULTS	35
4.1 Body mass and blood glucose in bariatric surgery patients	35
4.2 Body mass and body composition in SPF and GF mice after FMT from bariatric surgery patients	36
4.3 Blood glucose homeostasis in SPF and GF mice after FMT	37
4.3.1 Blood glucose homeostasis in SPF mice with BPD/DS FMT	37
4.3.2 Blood glucose homeostasis in SPF mice with VSL FMT	38
4.3.3 Blood glucose homeostasis in GF with BPD/DS FMT	38
4.3.4 Blood glucose homeostasis in GF with VSL FMT	39
4.4 Insulin and c-peptide levels in SPF and GF mice after FMT	40
4.5 Glucose transporter transcript levels in the intestine of SPF and GF mice after FMT	40
4.6 Glucose transporter transcript levels in the muscle, liver and adipose tissue of GF mice after FMT	41
4.7 GLUT1 protein level in the ileum of GF mice after FMT	42
4.8 Intestinal morphology in the duodenum/jejunum of GF mice after FMT	42
4.9 Intestinal morphology in the ileum of GF mice after FMT	43
5.0 DISCUSSION	44
5.1 Blood glucose homeostasis was improved in GF mice receiving post-surgery FMT	45
5.2 Changes in the expression of genes involved in intestinal glucose absorption was associated with improved glucose homeostasis in GF mice	46
5.3 Alteration in blood glucose homeostasis was associated with changes in the gut morphology of GF mice	48
5.4 Future directions	49
5.5 Limitations	52
6.0 CONCLUSION	54
7.0 REFERENCES	56

LIST OF FIGURES

Figure 1. Predominant locations of glucose transporters in the intestine area	69
Figure 2. Common types of bariatric surgery	70
Figure 3. Schematic of experimental design and methods	71
Figure 4. Body mass and blood glucose in bariatric surgery patients	72
Figure 5. Body mass and blood glucose in BPD/DS surgery patients	73
Figure 6. Body mass and blood glucose in VSL surgery patients	74
Figure 7. Changes in fasting blood glucose of selected patients undergone bariatric surgeries	75
Figure 8. Body features of female SPF mice received fecal microbiota from BPD/DS donors	76
Figure 9. Body composition of female SPF mice received fecal microbiota from BPD/DS donors	77
Figure 10. Body features of female SPF mice received fecal microbiota from VSL donors	78
Figure 11. Body composition of female SPF mice received fecal microbiota from VSL donors	79
Figure 12. Body features of female GF mice received fecal microbiota from BPD/DS donors	80
Figure 13. Body composition of female GF mice received fecal microbiota from BPD/DS donors	81

Figure 14. Body features of female GF mice received fecal microbiota from VSL donors	82
Figure 15. Body composition of female GF mice received fecal microbiota from VSL donors	83
Figure 16. Glucose curve and corresponding AUC in female SPF mice received fecal microbiota from BPD/DS donor	84
Figure 17. Glucose curve and corresponding AUC in female SPF mice received fecal microbiota from VSL donors	85
Figure 18. Glucose curve and corresponding AUC in female GF mice received fecal microbiota from BPD/DS donors	86
Figure 19. Glucose curve and corresponding AUC in female GF mice received fecal microbiota from VSL donors	87
Figure 20. Mice AUC blood glucose at week 7 plotted by donor	88
Figure 21. Insulin secretion of female SPF mice received fecal microbiota from BPD/DS donors	89
Figure 22. C-peptide secretion, ratio of insulin to c-peptide and HOMA-IR index of female SPF mice received fecal microbiota from BPD/DS donors	90
Figure 23. Insulin secretion of female GF mice received fecal microbiota from BPD/DS donors	91
Figure 24. C-peptide secretion, ratio of insulin to c-peptide and HOMA-IR index of female GF mice received fecal microbiota from BPD/DS donors	92

Figure 25. Glucose transporter mRNA expression in female GF mice received fecal microbiota from different bariatric surgery patients	93
Figure 26. Glucose transporter mRNA expression in female SPF mice received fecal microbiota from different bariatric surgery patients	94
Figure 27. Glucose transporter mRNA expression in female GF mice received fecal microbiota from different bariatric surgery patients	95
Figure 28. Representative blots	96
Figure 29. GLUT1/ α -actinin expression in the ileum of female GF mice received fecal microbiota from different bariatric surgery patients	97
Figure 30. Representative duodenum/jejunum histology images	98
Figure 31. Morphometric characteristics from the duodenum/jejunum segment of mice	99
Figure 32. Representative duodenum/jejunum histology images	100
Figure 33. Morphometric characteristics from the ileum segment of mice	101
Figure 34. Rate of 3-OMG absorption in female GF mice received fecal microbiota from BPD/DS patients	102

LIST OF TABLES

Table 1. Reagents used in the studies	24
Table 2. Antibodies used in the studies	25
Table 3. Primers used in RT-PCR	30

LIST OF ABBREVIATIONS

[¹⁸ F]FDG	[¹⁸ F]fluoro-D-glucose
3-OMG	3-O-methyl-glucose
AMPK	AMP-activated protein kinase
ANOVA	Analysis of variance
AUC	Area under curve
BMI	Body mass index
BPD	Biliopancreatic diversion
BPD/DS	Biliopancreatic diversion with duodenal switch
BSA	bovine serum albumin
ECL	Enhanced chemiluminescence
EWL	Excess weight loss
FFA	Free fatty acid
FMT	Fecal microbiota transplant
GF	Germ-free
GI	Gastrointestinal
GLP-1	Glucagon-like peptide 1
GLUT	Glucose transporter
GSIS	Glucose-stimulated insulin secretion
gWAT	Gonadal white adipose tissue
H&E	Haematoxylin and Eosin
HbA1c	Glycated hemoglobin
HFD	High fat diet
HOMA-IR	Homeostatic Model Assessment of Insulin Resistance
IFN- γ	Interferon-gamma
IL-4	Interleukin-4

IR	Insulin receptor
IRS	Insulin receptor substrate
JNK	c-Jun N-terminal Kinase (JNK)
MAP	Mitogen-activated protein kinase
mRNA	Messenger RNA
NAS	Non-caloric artificial sweetener
NFSM	Non-fat skim milk
oGTT	Oral glucose tolerance test
PBS	Phosphate buffer saline
PET/CT	Positron emission tomography-computed tomography
PYY	Peptide YY
RNA	Ribonucleic acid
RYGB	Roux-en-Y gastric bypass
SCFA	Short chain fatty acid
SEM	Standard error of mean
Ser	Serine
SLGT	Sodium-dependent glucose transporter
SPF	Specific-pathogen-free
T2D	Type 2 diabetes
TA	Tibialis anterior
TBS-T	Tris-buffered saline-Tween 20
Thr	Threonine
TNF- α	Tumor necrosis factor alpha
VSL	Vertical Sleeve Gastrectomy
WAT	White adipose tissue
WHO	World Health Organization

DECLARATION OF ACADEMIC ACHIEVEMENT

The following is a declaration that the content of the research presented in this thesis have been completed by Yuk Kwan Cassandra Chen, with some assistance from Dr. Fernando Forato Anhê with animal care. The research study was designed by Dr. Jonathan Schertzer, who also contributed to the review and completion of this thesis. All lab members from Schertzer lab contributed to blood and tissue collection for the mice samples. To the best of my knowledge, the content of this thesis does not infringe on the copyright of any others.

1.0 INTRODUCTION

1.1 *Obesity and type 2 diabetes*

The prevalence of obesity and its comorbidities is increasing in Canada and worldwide^{1,2}. The World Health Organization (WHO) defines obesity as a body mass index (BMI) over 30 kg/m², which is calculated by dividing body mass in kilograms by height in meters squared³. Obesity is characterized by increased fat mass, which is also associated with increased risk of multiple comorbidities including hypertension, cardiovascular disease and type 2 diabetes (T2D). In 2005, the prevalence rate of T2D in Ontario, Canada had exceeded the WHO'S predicted global prevalence rate for 2030⁴. According to the WHO, over 422 million of people now have diabetes worldwide, attributing to 1.6 million deaths annually, making this disease the seventh leading cause of death globally⁵. An analysis using the U.S. National Health Interview Survey data showed that the lifetime diabetes risk estimated at 18 years of age progressively increases from 7.6 to 70.3% for men and from 12.2 to 74.4% for women as body weight increases from underweight to very obese⁶. Analysis of over 114,000 U.S. women showed that the risk for T2D, independent of ethnicity, increased in direct association with increased BMI⁷ and this relation is consistent for any BMI greater or equal to 22 kg/m². Women with a BMI between 22.0 and 22.9 kg/m² have a 3-fold higher risk of T2D compared to women with a BMI lower than 22.0 kg/m². Overall, all these data show a strong correlation between obesity and T2D.

1.1.1 Mechanisms underlying insulin resistance, type 2 diabetes and obesity

Insulin, released from the pancreatic β -cells, normally functions to lower blood glucose level through suppression of hepatic glucose production and increased glucose uptake into muscle and adipose tissue among other peripheral tissues. The insulin signaling cascade initiates when insulin stimulates its membrane-bound cell-surface receptor. Insulin receptor (IR) contains an α -subunit that binds to insulin and the IR also contains a tyrosine-specific protein kinase β -subunit that responds to insulin binding⁸. Autophosphorylation occurs when phosphate groups are incorporated onto the β -subunit, which facilitate tyrosine phosphorylation of insulin receptor substrate (IRS) proteins. This promotes intracellular signal propagation, leading to increased cellular glucose uptake and suppression of hepatic glucose output, which are integrated responses that lower blood glucose.

Insulin resistance refers to a decreased ability of insulin to (i) lower hepatic glucose output and (ii) increase peripheral glucose uptake and storage⁹. Insulin resistance combined with β -cell dysfunction allows moderate glucose intolerance to progress to poorly controlled levels of fasting and post prandial blood glucose and eventually T2D¹. Modifications in the IR and IRS signaling cascade can lead to development of insulin resistance. A reduction in IR number, often termed IR down-regulation, can be associated with insulin resistance and can occur in mice with obesity and/or features of T2D⁹. Patients with loss-of-function mutations in IR can have severe insulin resistance, hyperglycaemia and hyperinsulinemia¹⁰.

IRS1-deficient mice have peripheral insulin resistance and moderate hyperglycaemia, leading to impaired skeletal muscle glucose uptake; while IRS2-deficient mice display insulin resistance with more profound hyperglycaemia^{11,12}. Phosphorylation of IRS1 at serine and threonine residues can inhibit tyrosine phosphorylation of IRS1, which impairs proper association with IR and signal propagation required to increase glucose uptake in peripheral cells¹³.

The ability of obesity to cause insulin resistance has been recognized for decades. There are several mechanisms that link obesity and insulin resistance. Plasma free fatty acids (FFAs), which inhibit insulin's action on glucose transport, are elevated in obese subjects due to increased FFA release and reduced FFA clearance from the expanded and stressed adipose tissue¹⁴. Elevated circulating FFAs can promote lipid deposition in peripheral tissues outside of adipose tissue. When FFAs are converted to excessive triglycerides in the liver, this is one factor that can promote hepatic insulin resistance. Elevated circulating FFAs can also lead to peripheral insulin resistance in skeletal muscle¹⁵. An excessive FFA load (or other mechanisms of cellular stress) can induce insulin resistance by activating serine phosphorylation of IRS1¹⁶. FFAs are potent activators of c-Jun N-terminal Kinase (JNK), a member of the mitogen-activated protein kinase (MAP) family that have been shown to promote serine phosphorylation of IRS1, particularly at Ser³⁰⁷, which inhibits IRS1 tyrosine phosphorylation and insulin signal propagation. Absence of JNK1 results in protection from obesity-induced

insulin resistance, while increased JNK activity promotes insulin resistance and indicators of T2D in mice¹⁷.

It is well established that adipose tissue volume is correlated with the level of insulin resistance¹⁸. Beyond FFAs and lipids, many other adipose-derived factors can influence obesity-related insulin resistance. Adipokines are cytokine-like endocrine factors that are secreted by adipose tissue and can function as proteins involved in lipid and glucose homeostasis¹⁹. Adipose tissue hypoxia, adipocyte stress and adipocyte necrosis are all associated with obesity and can alter adipokine profiles¹⁹.

Obesity also has a strong association with inflammation. Macrophages exist along a continuum of phenotypic profiles, but this can be simplified into two different types of macrophages in white adipose tissue (WAT). Proinflammatory M1 macrophages are recruited by proinflammatory cytokines that are produced by the expanded adipose tissues²⁰. M1 macrophage polarization in adipose tissue can further increase secretion of proinflammatory cytokines including tumor necrosis factor- α (TNF- α), which leads to more macrophage recruitment and an inflammatory response amplification. Interleukin-4 (IL-4) is one factor that polarizes macrophages into the anti-inflammatory M2 macrophages²⁰. M2 macrophages can dampen inflammatory responses and can secrete anti-inflammatory cytokines. Obesity can influence macrophage polarization. For example, adipose tissue expansion during obesity can lead to lower IL-4 receptor expression on M2 macrophages, which reduces the ability of M2 macrophages to

promote anti-inflammatory functions. In fact, lower IL-4 receptor expression promotes polarization into M1 macrophages²¹. The balance between IL-4 receptor expression and M2 versus M1 macrophage polarization can influence macrophage infiltration into adipose tissue and TNF- α levels. TNF- α is one proinflammatory factor that can polarize macrophages from M2 to M1 phenotypes in adipose tissue. TNF- α can also activate JNK and other serine kinases, which results in serine phosphorylation of IRS1, thereby promoting insulin resistance through a stress kinase mechanism of action. Several interventions including bariatric surgery can cause changes in adipokine secretion, reduce obesity-associated inflammation and mitigate hepatic and peripheral insulin resistance²². The mechanisms of bariatric surgery-induced changes in metabolism will be explained in the later sections.

1.1.2 Prediabetes and glucose metabolism

Prediabetes is characterized by a moderate elevation in fasting blood glucose, impaired glucose tolerance or both; however, the characteristics of prediabetic individuals do not yet meet the diagnostic criteria for diabetes²³. There are many underlying mechanisms linking obesity and alterations in glucose metabolism that are involved in the progression of pre-diabetes. The above-mentioned obesity-induced insulin resistance is one key mechanism of prediabetes progression. In addition, changes in the activity and expression level of glucose transporters and co-transporters involved in intestinal glucose

absorption and metabolism have been reported in individuals with impaired glucose tolerance. To date this work has been focused on *Glut1*, *Glut2*, *Glut3*, *Glut5* and *Sglt1*. *Glut1*, *Glut2*, *Glut3* and *Glut5* all belong to the facilitative glucose transporter family. Glucose transporter 1 (GLUT1) is expressed ubiquitously and plays a pivotal role in early life intestinal tissue growth²⁴⁻²⁶ (Figure1). GLUT1 is the major insulin-independent glucose transporter in tissues that dispose blood glucose such as skeletal muscle²⁷. GLUT1 is also thought to provide a pathway to transport glucose across the blood brain barrier. Preclinical models of bariatric surgery have shown to increase levels of GLUT1 in the intestine. For example, rats that have undergone Roux-en-Y bypass (RYGB)-like surgery have increased GLUT1 RNA and protein expression in the Roux limb compared to the sham-operated rats²⁶. These RYGB-treated rats are thought to exhibit a reprogramming of their intestinal glucose metabolism to meet the increased anabolic needs on intestinal tissue growth and maintenance.

To investigate how bariatric surgery impacts glucose uptake and metabolism, studies have used positron emission tomography-computed tomography (PET/CT) scanning with intravenous administration of 2-deoxy-2-[¹⁸F]fluoro-D-glucose ([¹⁸F]FDG) to assess glucose metabolism. FDG is transported into the cells via glucose transporters and is then phosphorylated by hexokinase to FDG-6-phosphate, which cannot be metabolized further and thus remains in the cell²⁸. When the rates of glycolysis and glucose transport of a cell is enhanced, it could lead to an increased uptake of FDG. RYGB increased

[¹⁸F]FDG uptake by the Roux limb in rats compared to the jejunum of sham-operated rats when [¹⁸F] FDG is administered intravenously²⁸. A role for GLUT1 was revealed using phloretin, a GLUT1 inhibitor, in RYGB-treated rats. Phloretin blunted [¹⁸F]FDG uptake by the Roux limb compared to the RYGB-treated rats without the administration of phloretin²⁶. Therefore, the higher intestinal glucose uptake in RYGB-treated rats is thought to be mediated through GLUT1.

GLUT2 is mainly found in liver cells and pancreatic β -cells, but it is still present at lower levels in the kidney and intestines. GLUT2 can transport the dietary-absorbed glucose from the enterocytes into the circulation and is the primary glucose transporter responsible for transporting glucose across the basolateral membrane of intestinal epithelial cells. It has also been suggested that GLUT2 is coupled with glucokinase function, and together this coordinated regulation leads to appropriate glucose sensing by β -cells^{29,30}. Recent studies in diabetic rats have found that GLUT2 can be inserted transiently into the apical membrane of the jejunum in response to high intestinal luminal glucose concentration. In fact, apical GLUT2 can provide a large component via facilitated transport, which can account for 75% of glucose absorption related to this method^{31,32}. However, these effects are only present in diabetic rats and insulin resistant mice, where a large number of GLUT2 has been found to be permanently located in the apical membrane of intestinal epithelial cells. Normally, blood insulin prevents the insertion of GLUT2 on the apical membrane

and limits glucose absorption even if the luminal glucose level is high in the absence of obesity and insulin resistance.

GLUT3 is present at various levels in most tissues, but mainly in the brain and neuronal tissues, where it transports glucose into the brain and peripheral nerves, which rely heavily on glucose as a fuel source. In fact, GLUT3 has a higher affinity for glucose than GLUT1, 2 or 4, with a fivefold greater transport capacity than GLUT1 and 4. In addition, GLUT3 deficiency can lead to a decrease in transplacental glucose transport and fetal glucose uptake³³. GLUT3^{-/-} mouse embryos have a similar phenotype to diabetic mouse blastocysts including significant growth retardation and failure to progress past embryonic day 6.5^{33,34}.

GLUT5 is expressed on the brush border membrane of enterocytes and is a fructose transporter³⁵. Fructose represents a large component of Western diets and fructose metabolism is believed to partially contribute to the rising incidence of insulin resistance³². In humans and rats, GLUT5 is capable of transporting both fructose and glucose; however, human GLUT5 is a relatively poor glucose transporter³⁶. In contrast to GLUT1, GLUT5 expression is much lower in fetal small intestine than in the adult. GLUT5 abundance is developmentally regulated with its highest level in adult small intestine³⁷. GLUT5 participates in the transepithelial fructose uptake by regulating the movement across the luminal surface of the enterocytes.

Sodium-dependent glucose transporter (SGLT)-1 is also localized in the small intestinal brush border membrane and is the major glucose transporter in gastrointestinal (GI) tract^{38,39}. SGLT1 mediates the uptake of dietary glucose from the intestinal lumen into the epithelial cells with Na⁺ co-transport, which depolarizes the membrane and stimulates Ca²⁺ entry. SGLT1-mediated Ca²⁺ intake enhances glucagon-like peptide 1 (GLP-1) secretion from intestinal cells, which augments post-prandial insulin secretion from pancreatic β -cells⁴⁰. Increased upper small intestinal SGLT1 expression correlated with increased upper small intestinal glucose uptake in rodents and human after treatment with the commonly used antidiabetic drug metformin⁴¹. Obesity caused by a high fat diet (HFD) feeding lowers SGLT1 expression in the upper small intestine of rats, which was mitigated with metformin treatment⁴¹. In addition, metformin can increase glucose-stimulated GLP-1 release and improve glucose sensing in the upper small intestine^{41,42}. However, other studies have shown contradictory results where inhibition of SGLT1 leads to reduced glucose absorption and increased release of GLP-1 and peptide YY (PYY) from the GI tract⁴³. Multiple studies have used LX4211, a dual SGLT1/SGLT2 inhibitor that improves glycemia and increases circulating levels of GLP-1 in patients with T2D^{43,44}. It has been hypothesized that LX4211-associated postprandial increase in GLP-1 may be mediated by a mechanism independent of SGLT1 and this could involve SGLT2.

1.2 Bariatric surgeries

Lifestyle interventions including changing dietary patterns and physical exercise can influence diabetes risk, but currently these approaches have failed to mitigate increased prevalence of obesity and diabetes⁴⁵. In fact, 80-90% of the population that start low-calorie diets have failed to maintain long-term weight loss⁴⁶. Drug therapy can help reduce complications of diabetes, but pharmacotherapies rarely put diabetes into remission⁴⁷. Currently, the most effective and durable treatment for obesity and its comorbidities is bariatric surgery⁴⁸. Bariatric surgery causes substantial and durable weight loss, which is a key factor that promotes T2D remission. However, studies in both rodents and humans have suggested that bariatric surgery can also cause direct, weight-independent effects on blood glucose and diabetes status⁴⁹⁻⁵¹. Bariatric surgery can induce rapid improvement of hyperglycaemia, reduction in hepatic insulin resistance and changes in food preference⁴⁶. For instance, patients who have undergone biliopancreatic diversion with duodenal switch (BPD/DS) surgery have reduced fat intake while RYGB patients have reduced sweet and fatty food intake along with increased vegetable consumption^{52,53}. Unlike non-surgical weight loss, it appears that bariatric surgery does not lead to increased hunger and reduced energy expenditure. Rather, bariatric surgery attenuates appetite despite having a reduced calorie intake⁴⁸. It is still unclear what feedback mechanisms, circulating factors and pathways influence energy balance and glucose metabolism after specific types of bariatric surgery. In particular, the factors that

promote blood glucose lowering, which may occur independent of weight loss after bariatric surgery, are still not well characterized.

1.2.1 Types of bariatric surgery

Bariatric surgery can be divided into two categories. Restrictive surgeries restrict patient's food intake (e.g. gastric banding, vertical sleeve gastrectomy (VSL)) while malabsorptive surgeries decrease a patient's food absorption (e.g. RYGB)⁴⁶.

Among all bariatric surgery types, gastric banding popularity has increased the most in recent years⁵⁴. Gastric banding is performed by placing adjustable/nonadjustable bands around the proximal aspect of the stomach immediately below the gastroesophageal junction (Figure 2 (a)⁵⁵). VSL is originally a part of the duodenal switch operation that resects the lateral aspect of the gastric body and fundus (Figure 2 (b)⁵⁵). Sleeve gastrectomy is performed to inhibit gastric acid secretion and best preserve normal gastric physiology. In RYGB, a gastric pouch is created below the gastroesophageal junction using a linear stapler (Figure 2 (c)⁵⁵). The distal jejunal limb is then brought up towards the gastric pouch, creating a Roux limb, which is carefully measured to anastomose the biliopancreatic limb of the jejunum. This Roux limb will be the primary recipient of food after bariatric surgery is performed. Duodenal switch is performed when duodenum is dissected 2-3cm distal to the pylorus, anastomosed to a 250-cm alimentary limb with a 100-cm common limb channel⁵⁶

(Figure 2 (d)⁵⁵). When combined with sleeve gastrectomy, this procedure is called BPD/DS, which is hypothesized to be the most effective bariatric surgery type for obese patients.

1.2.2 Impact of bariatric surgery on obesity

Different types of bariatric surgery can cause both rapid and durable weight loss. Gastric banding slows food consumption and reduces amount of food being consumed. VSL is performed to reduce patient's stomach size and therefore restricting food intake⁵⁴. RYGB is the most commonly performed bariatric surgery type, comprising 70% to 75% of all bariatric surgeries⁵⁴. It is performed to bypass the distal stomach, duodenum and the proximal jejunum. Consequently, food being swallowed will go into the gastric pouch and then directly into the small intestine, bypassing most part of the stomach. This leads to increased satiety and decreased food intake, which are thought to be mediated by gut hormones involved in satiety⁵⁷. BPD/DS is considerably the most complex operation among all types of bariatric surgery. Biliopancreatic diversion (BPD) delays the involvement of bile and pancreatic juice in digestion by shortening the absorptive intestinal surface. As a result, bile is kept away from its normal entrance at the gastric outlet, leading to increased risk of complications such as peptic ulcers in patients⁵⁸. Although side effects have been observed from patients that underwent BPD/DS, it remains to be the most effective bariatric surgery when treating obese patients. A study has found that the excess weight

loss (EWL) three years after bariatric surgery operation is $84.0\% \pm 14.5\%$ for BPD/DS patients and $63.7\% \pm 17.0\%$ for RYGB patients⁵⁹. Although the underlying mechanism is not fully understood, it is thought that the combination of reduced food ingestion, changes in food preference, increase in satiety, release of satiety-promoting gut hormones and a shift in bile acid metabolism altogether promotes weight reduction and improves energy balance in obese patients.

1.2.3 Mechanisms of bariatric surgery on type 2 diabetes remission

In a meta-analysis of 134 studies completed in 2004, it was found that T2D remission rate was 48% for patients that underwent laparoscopic adjustable gastric banding, 84% for those that underwent gastric bypass and 98% for those underwent BPD/DS⁶⁰. It is becoming clear that some of the effects of bariatric surgery on blood glucose control and cellular glucose metabolism are independent of weight loss, including mechanisms linked to insulin resistance. Many adipokines related to insulin resistance such as visfatin and vaspin change after bariatric surgery¹⁹. Visfatin binds non-competitively to the IR and activates insulin signaling pathway, increasing glucose uptake and promoting insulin sensitivity^{20,61}. Studies have found an elevated blood visfatin after bariatric surgery, which correlates with increased insulin sensitivity seen in patients. Another hormone, visceral adipose tissue-derived serine protease inhibitor (vaspin) is higher in the serum of T2D and overweight subjects when compared

to lean subjects. The exact mechanism of how vaspin plays a role in T2D and obesity is not yet clear. However, weight loss lowers serum vaspin and this correlated with decreased plasma insulin concentration and increased insulin sensitivity^{62,63}. Bariatric surgery and the associated weight loss also lower serum vaspin⁶⁴. However, caution is warranted in simply tracking changes in adipokines and weight loss after bariatric surgery. In fact, stratifying patients according to high and low vaspin levels before and after BPD/DS surgery found that vaspin may be a beneficial adipokine regarding insulin sensitivity and glucose control⁶⁵. It was shown that BPD/DS surgery lowered vaspin, but that having high (i.e. >2.5 ng/mL) vaspin before and after BPD/DS was correlated with lower insulin and blood triglyceride, and higher high density lipoprotein-cholesterol and insulin sensitivity compared to BPD/DS patients with low serum vaspin.

It has been found that bariatric surgery also alters gut hormones including PYY and GLP-1 that not only reduce appetite, food intake and body weight, but also mediate glycemia⁶⁶. Elevated fasting PYY levels have been reported in several gastrointestinal diseases that are associated with loss of appetite^{67,68}, which is interesting since bariatric surgery can influence these gut hormones and suppress appetite. Postprandial PYY and GLP-1 level start to rise as early as 2 days after RYGB⁶⁶. Moreover, patients with less weight loss after RYGB have lower postprandial PYY and GLP-1 levels compared to those with normal post-surgery weight loss⁵⁴. Inhibition of PYY and GLP-1 in RYGB patients results in return of appetite and increased food intake⁶⁶.

1.3 The intestinal microbiota

Gut microbiota refers to the trillions of bacteria that reside within the GI tract. This community of commensal bacteria influences digestibility and energy harvest from ingested food⁶⁹. In concert with weight reduction and the potential resolution of T2D, bariatric surgery alters the composition of the intestinal microbiota. In patients that have undergone RYGB, an increase in gut microbiota richness, the number of gut microbiota species, is observed^{70,71}. It is known that gastric banding and VSL can cause changes in the composition of gut microbiota^{72,73}. To date, there is little information on gut microbiota changes after BPD/DS. Given the change in gut anatomy after bariatric surgery, it is not surprising that the composition of the gut microbiota is different in the remaining section of the intestine. More importantly, it is thought that changes in the composition of the microbiota may have a functional impact on obesity and blood glucose after bariatric surgery.

1.3.1 Obesity, bariatric surgery and gut microbiota

Factors derived from the gut microbiota can influence host inflammatory, endocrine and metabolic responses and the connections therein. Obesity can alter the taxonomy of gut microbiome and studies suggested that gut microbiota from obese subjects has a greater capacity to extract energy from food, leading to energy excess, a characteristic of obesity⁷⁴. One 16S rRNA sequence analysis of obese subjects revealed that 75% of the obesity-enriched bacterial genes are

characteristic of Actinobacteria, while 42% lean-enriched bacterial genes are from Bacteroidetes⁷⁵. Children with increased susceptibility to obesity have shown to have alterations in the composition of gut microbiota in early life, even at 6 and 12 months of age⁷⁶. Studies have also found a reduction in *Bifidobacteria* and *Bacteroides*-related intestinal bacteria in obese subjects, which correlates with increased fat mass and body weight gain and diabetes⁷¹. Increased Enterobacteriaceae is also reported in morbidly obese human subjects^{75,77-79}. Overall, there is some evidence for decreased Bacteroidetes and increased Firmicutes and Actinobacteria in obese subjects when compared to lean subjects⁸⁰. There are many conflicting reports on obesity and specific obesogenic diets on the composition of the gut microbiome. For example, feeding rats an obesogenic HFD decreases the abundance of Actinobacteria phylum while increasing the abundance of Proteobacteria in the upper gut, as revealed by 16S rRNA sequencing⁴¹. There are many reasons why discordant effects of obesity and the composition of the gut microbiome may be reported, including technical aspects of sample preparation such as different DNA extraction methods and differences in taxonomic assignment in analysis pipelines. Also, environmental factors such as diet and the composition of macronutrients have a large effect on the composition of the gut microbiome and so do therapeutic drugs. Interestingly, metformin treatment can increase the low abundance of *Lactobacillus* in the upper small intestine of HFD rats while dominated *Lactobacillus* genus in the upper gut is a phenotype seen in lean

mice. It is clear that obesity and obesity-causing diets promote gut segment-dependent changes in the composition of the microbiome. However, alterations in gut microbiota composition have rarely been directly linked to functional outcomes in host metabolism. It is rather suggested that some of the potential mechanisms of action including the regulation lipid deposition in adipocytes and hepatocytes may be driven by microbial derived factors.

Consistent with altered gut microbiota seen in obese patients, changes in gut microbiota are also observed following weight loss. A significant reduction in fecal Enterobacteriaceae is observed in obese adolescents following substantial weight loss in response to a physical exercise program with energy-restricted diet⁸¹. In a similar study, obese adolescents that undertook a physical activity regime and calorie-restricted diet had an increased relative abundance of *Bacteroides/Prevotella* and elevated level of *Bifidobacteria* in their feces⁸². These findings are similar to changes in the composition of the gut microbiome observed in obese patients that have undergone bariatric surgery. These changes in microbial taxonomy may relate to metabolic activity of the gut microbiota and how it influences host metabolism possibly to reduce fat deposition, decrease absorption and utilization of carbohydrates as well as facilitate energy extraction from food and storing the calories in host adipose tissue⁷³.

Bariatric surgery clearly changes the gut microbiota composition. Bariatric surgery involves surgical rearrangement of the GI tract, which results in altered

nutrient presentation and changes in pH in various gut segments⁸³. These are potent influencers of microbial communities and the composition of the gut microbiota shifts in an effort to adapt to these changes in the intestinal environment. Studies have compared the gut microbiome of obese human subjects, before and after RYGB, and found a shift in the stool microbial community structure after the surgery was performed. A low proportion of *Bacteroides/Prevotella* ratio was found in the feces of obese subjects before RYGB, but this ratio was significantly increased 3 months after surgery⁷¹. It also appears that the increase in *Bacteroides/Prevotella* ratio was positively correlated with reduction in fat mass after RYGB⁷¹. In this study, it was proposed that the altered anatomy of the gastrointestinal tract may affect food digestion due to the reduced stomach and shortened small intestine, which is one factor that can result in the microbial population shift seen in the bariatric surgery patients⁷⁰. In another study where the fecal microbiota from patients after VSL and RYGB was analyzed, three major phyla changes were observed in RYGB patients one year after surgery operation when compared to their own gut microbiota before the surgery⁸⁴. Specifically, increases in the relative abundance of Firmicutes and Actinobacteria and a decrease in Bacteroidetes were observed after RYGB. VSL patients also had increased relative abundance Bacteroidetes in the fecal microbiota one year after VSL surgery.

The composition of gut microbiota is closely related to development of obesity. However, the directionality in the relationship between bariatric surgery, microbiota and metabolic status of the host is not yet clear.

1.3.2 Effects of gut microbiota on blood glucose

There is evidence that the composition of the gut microbiota is altered in T2D, but this is often difficult to separate from the effects of obesity. For example, a reduction in the abundance of *Faecalibacterium prausnitzii* is reported in both obese and diabetic patients. T2D associated gut microbiota is enriched in functions involved in sugar transport⁸¹. In a study comparing germ-free mice to mice born germ free, but then colonized with the gut microbiome derived from conventional (non-germ-free) mice, the colonized mice were observed to have a 60% increase in fat mass and show indicators of reduced insulin sensitivity within two weeks of colonization⁸⁵. This phenomenon in mice is accompanied by an increase in the intestinal glucose absorption as well as higher glycemia and insulinemia, two key metabolic factors promoting lipogenesis⁶⁹.

Several probiotic strategies have been proposed to lower blood glucose and it has been demonstrated that plasma glucose level can be lowered through oral administration of heat-killed *Lactobacillus casei* strain Shirota in mice⁸⁶. Prebiotic treatment with inulin-type fructans can induce changes in gut microbiota, modulate gut hormones including GLP-1 and PYY, which provide some evidence that prebiotics may mediate satiety and hunger sensation,

promote weight loss and improve glucose regulation⁸⁷. Conversely, administering specific antibiotics can lower blood glucose and improve glucose control in obese mice^{88,89}.

It is well established that gut microbiota plays a role in immune system development⁹⁰. T2D can compromise aspects of gut barrier function and increase intestinal permeability to microbial derived factors that can activate inflammatory pathways and increase inflammation in metabolic tissues. This is one way that T2D can lead to inflammation and insulin resistance in insulin responsive tissues via stress responses and serine phosphorylation of IRS-1⁸⁰.

In addition, gut microbes can alter metabolism through generation of metabolic by-products, such as short chain fatty acids (SCFAs). These bacterial-derived metabolites are produced by fermentation and can have beneficial or deleterious effects on host metabolism depending on the dose and metabolic process studied. SCFAs such as butyrate and acetate can help maintain epithelial barrier function and reduce intestinal permeability⁹¹. The SCFA butyrate can increase fatty acid oxidation and energy expenditure while decreasing body weight in humans⁹². Other studies have shown that butyrate can influence host appetite, energy extraction and absorption from the diet^{93,94}. Oral administration of butyrate induces anti-inflammatory regulatory T cells, which can decrease macrophage infiltration in adipose tissue and improve insulin sensitivity⁹². Conversely, the microbial derived SCFA acetate can activate a parasympathetic

response that increases appetite, insulin levels and promotes the processes involved in T2D progression in mice⁹⁵.

2.0 RATIONALE, HYPOTHESES AND RESEARCH AIMS

2.1 Rationale

Bariatric surgery induces weight loss, leads to T2D remission and alters the composition of gut microbiota in both humans and animals. However, whether the change in the gut microbiota within a human patient is a standalone factor altering glucose metabolism has not yet been confirmed. The purpose of the present study is to examine the effect of the gut microbiota on blood glucose in mice that are exposed to the bacterial communities present in the feces of patients before and after bariatric surgery. Understanding the mechanisms of how the gut microbiota contributes to improving blood glucose homeostasis may allow for new insights in designing therapies to lower blood glucose and combat T2D.

2.2 Hypothesis

We hypothesize that transplantation of the fecal microbiota from patients that have undergone BPD/DS or VSL bariatric surgery will lower blood glucose in mice. Furthermore, we hypothesize that transplantation of the abovementioned fecal microbiota would alter gut-mediated glucose metabolism, which would be demonstrated by a lower glucose transporter expression in the intestine and altered intestinal architecture indicated by lower villus height, crypt depth and goblet cell number in the upper gut.

2.3 Research aims

Using fecal material obtained from female bariatric surgery patients and female conventional (specific-pathogen-free, SPF) and female germ-free (GF) BL6/NTac mice fed with CHOW diet, our research objectives were:

- 1) To investigate the role of the gut microbiota from human donors before and after bariatric surgery on glucose homeostasis in mice.
- 2) To determine if bariatric surgery-induced changes in the gut microbiota alter insulin secretion and/or the protein levels and the expression of genes involved in intestinal glucose absorption and metabolism.
- 3) To investigate the role of the gut microbiota from human donors before and after bariatric surgery on intestinal morphology in the duodenum/jejunum and ileum.

3.0 EXPERIMENTAL METHODOLOGY

3.1 Reagents and antibodies

For a full list of reagents and antibodies used, please refer to details contained in Table 1 and Table 2.

Table 1. Reagents used in the studies

Reagent	Manufacturer	Reagent	Manufacturer
10X PCR Gold buffer	Applied Biosystem	Isopropanol	VWR
5X SSIV buffer	Invitrogen	methanol	VWR
Acetic acid, glacial	Caledon	MgCl ₂	Applied Biosystem
Acrylamide	Fisher Bioreagent	Molecular grade water	Mediatech
Albumin	Bioshop	NaCl	Bioshop
Ammonium persulfate	Sigma	NaF	Sigma
Amplitaq Gold	Applied Biosystem	Non-fat skim milk	Selection
Anhydrous Ethanol	Fisher Scientific, Commercial Alcohol	Oligo-dt(18)	McMaster Mobix Lab
BCA Pierce	Thermo Scientific	oligonucleotide primer	McMaster Mobix Lab
BSA	Bioshop	PBS	Thermo Fisher
chloroform	Anachemia	Pouceau S stain	VWR
dithiothreitol (DTT)	Invitrogen	Protease Inhibitor Cocktail Tablet	Roche
DNase I 10x Reaction buffer	Invitrogen	random hexamers	McMaster Mobix Lab
DNase I Amplification grade	Invitrogen	random pentadecamers	McMaster Mobix Lab
dNTP (dATP, dTTP, dGTP, dCTP)	Wisent Bio Product	SDS	Sigma Aldrich
ECL	BioRad	stripping buffer	VWR
EDTA	Sigma	Superscript IV	Invitrogen

Reagent	Manufacturer	Reagent	Manufacturer
Glucose	Sigma	TEMED	BioRad
Glycine	Bioshop	Tris Base	Bioshop
HCl	Caledon	Triton-X	Sigma
HEPES	Sigma	TriZOL	VWR Chemical
Homogenizer ceramic beads	Omni International	Tween-20	Sigma

Table 2. Antibodies used in the studies

Primary antibody	Dilution	Catalogue number	Manufacturer
GLUT1	1:1000	ab115730	Abcam
α -actinin	1:1000	N/A	N/A

3.2 Animal care and tissue collection

The McMaster University Animal Ethics Review Board approved all procedures. Female SPF and GF BL6/NTac mice were originally sourced from Taconic and bred in the Central Animal Facility (CAF) at McMaster University. Female mice aged between 8 and 11 weeks were fed with *ad libitum* access to standard CHOW diet and water. The CHOW diet used in all studies was Teklad's irradiated global 18% protein rodent diet (2918). A schematic diagram of the study design is included in Figure 3. Experiments were conducted by transferring fecal materials from each human donors into either four SPF mice that have an established microbiota or four GF mice that lack gut bacteria. Fecal materials from three human donors were included in each study.

Human patients were enrolled in the bariatric surgery care centre of the Institut Universitaire de Cardiologie et de Pneumologie de Québec, Université Laval (IUCPQ) according to the institutionally approved management procedures. Ethical approval was granted by the Canadian Institute of Health and Reach, policy no. 2017-2746 21386. All participants provided written informed consent. Human fecal samples from VSL and BPD/DS types of bariatric surgery were collected before and after a 12-month follow-up and frozen immediately at -20 °C and subsequently stored at -80 °C. Three patients that had undergone BPD/DS and three patients that had undergone VSL were selected based on the largest reduction in fasting blood glucose at the 12-month follow-up compared to fasting blood glucose before each surgery type and it was ensured that these patients had not used antibiotics. The frozen donor fecal sample was prepared 1:10 (w:v) with PBS. The solution was mixed well and quickly spun at 1,500g. The supernatant was pipetted, aliquoted and stored at -80°C for future use. In total, fecal microbiota transplantation (FMT) were completed in 4 separate cohorts.

Two studies were completed with GF mice, one experiment with FMT to GF mice from three BPD/DS donors, one experiment with FMT to GF mice with three VSL donors. Another two mouse studies were completed using SPF mice receiving FMT from the same BPD/DS and VSL fecal donors. FMT was conducted for 9 weeks by gavaging 3 times per week of 200 µL of the fecal material into 4 GF or 4 SPF mice from each patient selected (n=12). Autologous

FMT in a group of SPF mice was also conducted to serve as a control group (n=12). The same experiment protocol was applied to all four cohorts. Individual body weight and food intake per cage were measured weekly. At weeks 0, 3 and 7, body composition was examined using Bruker's minispec Whole Body Composition Analyzer LF 90II. At week 3 and week 7, oral glucose tolerance test (oGTT) was performed after a 6-hour fast. Mice were gavaged with 4 g/kg glucose solution equal to 10% of their body weight. Venous blood glucose was obtained at 0, 20, 30, 40, 60, 90 and 120 minutes. A glucose-stimulated insulin secretion (GSIS) test was conducted at week 8 after a 12-hour overnight fast. Mice were gavaged with 4 g/kg glucose solution equal to 10% of their body weight. At 0, 10, 60 and 120 minutes, blood glucose levels were measured using the Accu-Chek or Medisure glucometer. A full capillary tube (maximum volume: 70 μ L) of blood was also collected at 0, 10, 60 and 120 minutes post glucose (4 g/kg) gavage into a 1.5 mL Eppendorf tube containing 7 μ L of Protease Inhibitor Cocktail and 1.75 μ L of DPP4 inhibitor with EDTA. Serum was obtained by centrifuging the blood at 16,260 x g for 10 minutes at 4 °C using the Eppendorf Centrifuge 5804 R and storing at -80 °C until further use. At week 9 of each study after a 12-hour overnight fast, whole blood was obtained by facial bleeding and serum was collected. Mice were then subsequently euthanized using cervical dislocation, with tissues harvested (liver, gonadal white adipose tissue (gWAT), inguinal white adipose tissue (iWAT), spleen, pancreas and tibialis anterior (TA) muscles), weighed and snap frozen in liquid nitrogen. Luminal contents from

intestinal segments were separated from host tissues (duodenum/jejunum, ileum, cecum with luminal content, colon), harvested and snap frozen in liquid nitrogen. All samples were stored at -80 °C until needed.

3.3 Serum analyses

The serum samples obtained after GSIS were analyzed by a postdoctoral fellow, Dr. Fernando Anhô, using Multiplex Immunoassays to quantify insulin and c-peptide. The protocol is adapted from *Foley et al*⁹⁶.

3.4 Gene expression analysis

3.4.1 RNA extraction

Approximately 30 mg of each tissue was homogenized in 0.9 mL TRIzol® using ceramic beads. Homogenization was performed using MP Biomedical's FastPrep-24™ Classic Instrument at 5 m/s for 60 seconds for three cycles. For isolating RNA from gWAT, a slight modification was used where 100 mg of starting material was obtained, homogenized, centrifuged for 10 minutes at 16,260 x g at 4 °C, and the supernatant was transferred to a new tube before initiation of the extraction process. Subsequently, for all sample tissues, 300 µL of chloroform was added and samples were vortexed, mixed well and incubated at room temperature for five minutes. Each sample was then centrifuged at 16,260 x g for 10 minutes at 4 °C. The upper aqueous phase was transferred into a fresh tube containing 500 µL isopropanol to precipitate RNA. The sample was mixed well and incubated at room temperature for 20 minutes. Followed by a 10-minute

centrifugation at 16,260 g, 4 °C, the supernatant was discarded, and the RNA pellet was washed twice with 75% ethanol. The pellet was spun down after each wash at 16,260 x g for 5 minutes at 4 °C. Following the last wash, remaining ethanol was allowed to evaporate before dissolving the RNA pellet in UltraPure distilled water that was pre-heated to 55 °C. The sample was incubated at 55 °C for 15 minutes using the VWR Hybridization Oven. RNA concentration was measured by spectrophotometry, using Biotek Nanodrop Synergy H4 Hybrid Reader. The samples were equalized to 250 ng/μL and stored at -80 °C.

3.4.2 cDNA synthesis

For each sample, 1 μg of the RNA was mixed with 0.5 μL of DNase I 10x Reaction buffer and 0.5 μL DNase I Amplification grade for 15 minutes at room temperature to eliminate single- and double-stranded DNA from the samples. Subsequently, 0.5 μL of EDTA (25mM), 0.5 μL of dNTP (10mM) and 0.5 μL of random hexamer primer (250 ng) were added to each sample. The sample was incubated in the SimpliAmp Thermal Cycler (Applied Biosystems) at 95 °C for 10 minutes to inactivate DNase I and 55 °C for 10 minutes to anneal the cDNA synthesis primer. cDNA was synthesized by adding 2 μL of 5X SuperScript™ IV buffer, 0.5 μL of DTT (0.1M), 0.5 μL of UltraPure distilled water and 0.5 μL of Superscript™ IV to each sample. Each sample was incubated in the thermal cycler at 55 °C for 10 minutes and 80 °C for 10 minutes. cDNA was diluted 1:10

in UltraPure distilled water and stored at -20 °C for all samples except for the BPD/DS GF samples, which was diluted 1:25.

3.4.3 RT-PCR Reactions

For BPD/DS GF mice samples, 10 µL of each cDNA sample was mixed with 10 µL of the master mix (per sample: 5.1 µL UltraPure water, 2 µL 10X PCR Gold buffer, 2 µL MgCl₂, 0.4 µL dNTP (10 mM), 0.4 µL primer and 0.1 µL AmpliTaq® Gold). For a full list of commercial TaqMan primers used, refer to Table 3. RT-PCR was performed using Rotor-Gene Q (Qiagen), at 95°C for 10 seconds, then 58 °C for 45 seconds for 50 cycles. All genes were normalized to the housekeeping gene *Rn18S* using the $2^{-\Delta\Delta CT}$ method, using the pre-surgery mice group as the control condition. For all other samples, 15µL of the cDNA sample was added to 5 µL of the master mix, using 0.1 µL UltraPure water to compensate for the sample volume.

Table 3. Primers used in RT-PCR

Primer	Gene	Catalogue Number	Manufacturer
Rn18S	Rn18S	Mm03928990_g1	ThermoFisher
GLUT1	Slc2a1	Mm0044180_m1	ThermoFisher
GLUT2	Slc2a2	Mm00446229_m1	ThermoFisher
GLUT3	Slc2a3	Mm004414983_m1	ThermoFisher
GLU5	Slc2a5	Mm00600311_m1	ThermoFisher
SGLT1	Slc5a1	Mm00451203_m1	ThermoFisher

3.5 Protein Analysis

3.5.1 Protein Extraction from tissues

Approximately 20mg of intestine was lysed in SBJ lysis buffer (50 mM HEPES, 150 mM NaCl, 100 mM NaF, 10 mM NaP₂O₇, 5mM EDTA·2H₂O and 250 mM sucrose) supplemented with 1% Triton-X and a quarter tablet of protease inhibitor cocktail. Subsequently, 10 µL of lysis buffer was used per 1 mg of sample tissue with 2 homogenizer compatible ceramic beads. Homogenization was performed using FastPrep-24™ Classic Instrument twice at 4.5 m/s for 30 seconds. The samples were centrifuged for 15 minutes at 16,260 x g at 4 °C and the supernatant was transferred to a new tube and stored at -80 °C until needed.

3.5.2 Total Protein Measurements

Protein concentrations were measured by bicinchoninic acid (BCA) assay. Lysate samples were diluted 1:5 in Milli-Q® water and serially diluted protein standards were calculated using 2 mg/mL albumin standard diluted in Milli-Q® water. The protein concentration assay was run using a clear 96-well plate. Followed the protocol outlined by Pierce, the BCA working reagent solution was prepared by mixing Reagent A and Reagent B in a 50:1 ratio and 0.2 mL of the working reagent was added to each sample. All samples were run in triplicates, incubated at 37 °C for 30 minutes, and absorbance measures set at 562 nm were obtained using the Synergy H4 Hybrid Reader. Total protein concentration values were interpolated using Prism 8.0 software, based on the standard curve generated.

3.5.3 Immunoblotting

In contrast to standard immunoblotting techniques, samples were not heated to avoid the possible irreversible aggregation of glucose transporters⁹⁷. Protein lysates were prepared by adding 4X Laemmli buffer (8% SDS, 40% glycerol, 240 mM Tris HCl (pH 6.8), 10% 2-mercaptoethanol and 0.02% bromophenol blue) and dithiothreitol (DTT) was added to lysates. 15 µg of protein was loaded onto a 10% SDS-PAGE gel and electrophoresis was carried out at 112 V for 1 hour and 20 minutes. Proteins were transferred onto polyvinylidene fluoride membranes using the Trans-Blot Turbo System (bio-Rad) set at 25V for 28 minutes. Ponceau S staining was performed to confirm equal loading and imaged using Bio-Rad Image lab. Membranes were cut at the 75 kDa mark. The upper parts of the membrane (protein size > 75 kDa) were blocked in 3% bovine serum albumin (BSA) for 1 hour. The lower parts of the membranes (protein size < 75kDa) were blocked in 5% non-fat skim milk (NFSM) for 1 hour. All membranes were then incubated with primary antibodies overnight at 4 °C. All primary antibodies and their respective dilutions are listed in Table 2. Membranes were washed in Tris-buffered saline with 0.5% Tween-20 (TBS-T) for 4 times, each for 15 minutes. Membranes were then incubated with the horseradish-peroxidase-conjugated anti-Rabbit IgG secondary antibodies. Secondary antibodies were diluted 1:10000 in 5% NFSM in TBS-T for the upper parts of the membranes and 1:10000 in 3% BSA in TBS-T for the lower parts of the membranes. Membranes were incubated for 1 hour at room temperature and

washed four times for 15 minutes each. Enhanced chemiluminescence (ECL) solution was prepared according to manufacturer directions and membranes were incubated in ECL solution for 5 minutes before detection on the Bio-Rad Imager. Band intensities were quantified using Bio-Rad Image Lab and the data was exported to ImageJ and Prism 8.0 software for further analysis.

3.6 Histology

3.6.1 Hematoxylin and Eosin Staining

Duodenum/jejunum, ileum, cecum and colon were immersed in Carnoy's solution (6 mL ethanol, 3 mL chloroform and 1 mL glacial acetic acid) for a 3-hour fixation and arranged using the Swiss-rolling technique. The intestines were then washed with 100% ethanol 3 times and immersed in 70% ethanol for 72 hours. Afterwards, samples were sent to McMaster Histology department and 5 μ m cross sections were cut and mounted onto slides stained with hematoxylin and eosin (H&E) to visualize intestinal architecture and subsequently analyzed to for cross sectional morphology. One slide was prepared from each intestine segment from each mouse.

3.6.2 Image analyses

Images of H&E stained slides were acquired with a Nikon Eclipse Ni & DS-QI2 microscope and analyzed using NIS-Elements COLOUR. Nikon software was used to define the borders of the intestinal cross section, and three 10x magnification images and six 20x magnification images were taken from each

slide. All slide images were exported to Image J for further analysis. Villus height, villus width and muscular layer thickness in the duodenum/jejunum and ileum slides were measured using the three 10x magnification images. Goblet cell count and crypt count in the duodenum/jejunum and ileum slides were measured using the six 20x magnification images. Crypt depth in the duodenum/jejunum was measured using the 10x magnification images while crypt depth in the ileum was measured using the 20x magnification images.

3.7 Statistical analyses

Statistical analyses were carried out using Prism 8.0 software. Two-tailed unpaired, nonparametric Mann-Whitney tests were used to determine differences in two groups. For example, Mann-Whitney tests were used to compare the mean body mass between the pre-surgery and post-surgery GF mice. One-way analysis of variance (ANOVA) was used to determine differences among three groups. For example, one-way ANOVA was used to compare the total food intake among the autologous, pre-surgery and post-surgery SPF mice. Two-way ANOVAs were used to determine significant interaction between multiple means. For example, repeated measures ANOVA was used to compare the blood glucose level at different time points during the oGTT tests for all four animal studies. All results including the clinical data are expressed as mean \pm SEM (standard error of the mean) with a $p < 0.05$ considered significant.

4.0 RESULTS

4.1 Body mass and blood glucose in bariatric surgery patients

We aimed to test whether alterations in the gut microbiota of human patients after bariatric surgery was a standalone factor altering glucose metabolism in mice. We used frozen fecal samples from the same patient before and after two different types of bariatric surgery. The fecal samples used and the patient data analyzed were collected by the Quebec Heart and Lung Institute at Laval University on patients before and after a 12-month follow-up for VSL and BPD/DS types of bariatric surgery. These data showed that severely obese patients undergone BPD/DS or VSL bariatric surgeries both had significantly lower body mass, fasting blood glucose and glycated hemoglobin (HbA1c) % when tested at 4 and 12 months after the surgery (Figure 4). Patients that underwent BPD/DS type of surgery had lost significantly more weight and had a greater lowering of HbA1c levels at 12 months, compared to those that had VSL surgery. Individual patient's body mass, fasting blood glucose and HbA1c levels are shown after BPD/DS (Figure 5) and VSL (Figure 6). We then selected three patients that had undergone BPD/DS and VSL based on maximal reduction in fasting blood glucose at 12-month follow-up for each surgery type and ensured that these patients had not used antibiotics (Figure 7).

4.2 Body mass and body composition in SPF and GF mice after FMT from bariatric surgery patients

Both types of bariatric surgery reduced body weight and lowered blood glucose. We next used fecal samples from patients before and after both types of bariatric surgery to colonize mice in order to directly test if bariatric surgery-induced changes in the fecal microbiota could alter blood glucose (Figure 3). We conducted FMT by gavaging (3 times per week) the fecal samples from **each** patient into 4 GF or SPF mice. Importantly, this was done for 4 GF and 4 SPF mice from each patient selected in Figure 7 equating to n=12 mice per group. We also conducted autologous FMT in a group of SPF mice. We determined whether body mass and body composition changed in the recipient mice. Preliminary data collected by lab member Dr. Anhê showed that the percentage gain in body mass up to 8 weeks after FMT, as well as the total food intake, were not different in SPF mice with FMT from BPD/DS bariatric surgery patients (Figure 8). Body composition measured at week 7 revealed that all the SPF mice that had FMT from BPD/DS surgery had no difference in the fat, lean and fluid mass (Figure 9). Furthermore, in SPF mice with FMT from VSL patients confirmed all of these findings, showing no differences in body mass, body composition or food intake (Figure 10, 11). Similarly, performing the same FMT procedures from the same VSL and BPD/DS patient samples in GF mice, showed no significant differences in body mass, body composition or food intake (Figure 12-15). Overall, the data

revealed that FMT from VSL or BPD/DS patients did not alter body mass, body composition or food intake when transferred to either SPF or GF mice.

4.3 Blood glucose homeostasis in SPF and GF mice after FMT

We found that FMT from VSL or BPD/DS patients did not alter body mass or body composition in mice, which allowed us to test if the microbiota could alter blood glucose without changes in body mass. We conducted oGTTs in SPF and GF mice at 3 and 7 weeks after FMT, which allowed us to examine if FMT from bariatric surgery patients altered glucose homeostasis. Specifically, we tested if the duration of colonization could dictate changes in glycemia, where we have previously shown that at least ~40 days post FMT is required to alter blood glucose using FMT between mice⁸⁹.

4.3.1 Blood glucose homeostasis in SPF mice with BPD/DS FMT

Data collected by Dr. Anhê showed that three weeks after colonization of SPF mice using FMT from BPD/DS patients, mice that received FMT from the post-surgery group exhibited significantly lower blood glucose at 20 minutes during the oGTT compared to the pre-surgery group (Figure 16A). However, this did not translate into an overall lower AUC for the post-surgery group (Figure 16B). Seven weeks after colonization of SPF mice using FMT from BPD/DS patients, the data showed no difference among the three groups at any time points during oGTT and the AUC was similar for all the groups (Figure 16C, 16D).

4.3.2 Blood glucose homeostasis in SPF mice with VSL FMT

Three weeks after colonization of SPF mice using FMT from VSL patients, the data showed that the post-surgery group had lower blood glucose at 20 and 30 minutes during the oGTT compared to the autologous and pre-surgery group (Figure 17A). Nevertheless, the total AUC during this oGTT was not different between the pre- and post-surgery groups, but only for the autologous and pre-surgery groups (Figure 17B). Seven weeks after colonization of SPF mice using FMT from VSL patients showed that the AUC during the oGTT was similar for all three groups and only a significant difference between the autologous and the pre-surgery group 30 minutes during the oGTT was observed. These data suggested that FMT from the same patients obtained before and after two types of bariatric surgery was not able to robustly alter blood glucose during an oral glucose challenge in SPF mice.

4.3.3 Blood glucose homeostasis in GF with BPD/DS FMT

We next determined changes in glycemia after FMT in GF mice. Data on GF mice with FMT from BPD/DS patients showed no difference in blood glucose at specific time points and no difference in the AUC during the oGTT when tested at three weeks after FMT (Figure 18A, 18B). However, data obtained seven weeks after this colonization showed that the post-surgery group had significantly lower blood glucose at 30 minutes during the oGTT and AUC for blood glucose

was also significantly lower compared to mice that had pre-surgery FMT (Figure 18C, 18D).

4.3.4 Blood glucose homeostasis in GF with VSL FMT

FMT from VSL patients into GF mice demonstrated similar results (Figure 19). No difference was seen three weeks after colonization using FMT from VSL patients (Figure 19A, 19B). However, the post-surgery group had a significantly lower blood glucose at 40 minutes during the oGTT and a lower AUC for blood glucose when tested seven weeks after colonization using FMT from VSL patients. These data showed that when GF mice were colonized for an adequate amount of time, bariatric surgery-induced changes in gut microbiota was an independent factor that was sufficient to improve glucose control during an oral glucose challenge.

We tested 4 GF mice for each fecal sample obtained from a given patient before and after bariatric surgery. Hence, we wanted to determine if changes in blood glucose were driven by the response from a single human donor or if each donor produced a consistent response in changing blood glucose in mice. Therefore, we next analyzed the AUC of blood glucose during the oGTT for GF mice colonized for seven weeks and stratified the results by each human donor. The values obtained from mice colonized by the three donors selected for each surgery type showed comparable responses (Figure 20). Therefore, we

confirmed that microbiota-transmissible changes in blood glucose in GF mice was not driven by a single or subset of donors.

4.4 Insulin and c-peptide levels in SPF and GF mice after FMT

We found that transfer of the microbiota in fecal samples after bariatric surgery lowered blood glucose during an oGTT when conducted 7 weeks after FMT in GF mice. However, the mechanisms contributing to FMT-induced changes in glucose homeostasis remained ill-defined. To further investigate on whether bariatric surgery-induced changes in gut microbiota altered insulin secretion and insulin sensitivity and led to lower blood glucose, we quantified insulin and c-peptide in the serum of GF and SPF mice after FMT from pre- and post-surgery BPD/DS patients. The data showed no differences in insulin and c-peptide levels in SPF or GF mice (Figure 21, 22A, 22B, 23, 24A, 24B). In order to further examine on β -cell function and insulin resistance, HOMA-IR index was calculated using the formula “(fasting insulin [mUI/mL] x fasting glucose [mmol/L]) /22.5”. The HOMA-IR index was not different in SPF or GF mice after FMT from pre- and post-surgery BPD/DS patients (Figure 22C, 24C).

4.5 Glucose transporter transcript levels in the intestine of SPF and GF mice after FMT

We found that transfer of the microbiota in fecal samples after bariatric surgery lowered blood glucose during an oGTT, but FMT did not alter indices of insulin secretion or insulin sensitivity. We next investigated whether bariatric

surgery-induced changes in gut microbiota altered mechanisms of intestinal glucose absorption. We assessed the expression levels of *Glut1*, *Glut2*, *Glut3*, *Glut5* and sodium-dependent glucose co-transporter 1 (*Sglt1*) in the duodenum/jejunum, ileum and colon segments of GF mice. FMT using fecal samples before and after BPD/DS and VSL into GF mice showed that post-surgery FMT resulted in decreases in the transcript level of *Glut1* in the ileum of mice (Figure 25B, 25E). *Glut2* transcript levels decreased in the duodenum/jejunum of GF mice with VSL post-surgery FMT, but this was not seen in those with BPD/DS FMT (Figure 25A, 25D). Glucose transporter transcript levels were not significantly different in the colon of GF mice after FMT from either surgery type (Figure 25C, 25F). We next measured *Glut1* and *Glut2* transcript levels in the duodenum/jejunum and ileum segments of SPF mice, and no difference was observed (Figure 26). However, it was not yet clear whether these changes in *Glut1* were localized to the intestine, and whether this change could translate to GLUT1 protein level.

4.6 Glucose transporter transcript levels in the muscle, liver and adipose tissue of GF mice after FMT

We next determined whether changes in the transcript level of *Glut1* was reflected in other tissues of the mice. *Glut1* was measured in the liver, gonadal white adipose tissue (gWAT) and tibialis anterior (TA) muscle in GF mice that received FMT from patient samples obtained before and after BPD/DS and VSL. These data showed that *Glut1* was not different in the liver and gWAT tissues.

However, GF mice that received FMT from post-surgery BPD/DS donors had significantly higher *Glut1* transcript level in the TA muscle (Figure 27). Therefore we showed that changes in the transcript level of *Glut1* was not localized to the intestine, and that bariatric surgery-induced changes in the microbiota can decrease *Glut1* transcript levels in the upper intestine and increase *Glut1* transcript levels in the hindlimb skeletal muscle.

4.7 GLUT1 protein level in the ileum of GF mice after FMT

Western blotting was performed for immunoreactive GLUT1 in the ileum from GF mice that received FMT before and after BPD/DS and VSL (Figure 28). No significant difference was found in the relative amounts of GLUT1 protein between groups (Figure 29), indicating that gut microbiota altered by bariatric surgery was not able to translate changes to the protein level of GLUT1.

4.8 Intestinal morphology in the duodenum/jejunum of GF mice after FMT

We next investigated whether bariatric surgery-induced changes in gut microbiota altered the morphology of upper intestine segments of GF mice with FMT from BPD/DS donors. H&E (Haemotoxylin and Eosin) staining of transverse sections of duodenum/jejunum displayed no overt visual differences between GF mice that received FMT from the pre- and post-surgery samples (Figure 30). Mean villus height, villus width, muscle layer thickness and crypt depth were not significantly different in the duodenum/jejunum of these GF mice either (Figure 31A, 31C-31E). However, the number of goblet cells per 10 crypts was

significantly decreased in GF mice with post-surgery FMT from BPD/DS patients (Figure 31B).

4.9 Intestinal morphology in the ileum of GF mice after FMT

H&E stained sections of the ileum were also analyzed from GF mice with FMT from BPD/DS patients. Mean villus width and muscle layer thickness were not significantly different in the ileum of GF mice that received FMT from pre- and post-surgery samples (Figure 32, 33C, 33D). Similar to the H&E stained sections of duodenum/jejunum, the mice with post-surgery FMT showed decreased number of goblet cells per 10 crypts (Figure 33B). However, the ileum of GF mice with post-surgery FMT also had lower mean villus height and crypt depth, compared to those that received FMT from the pre-surgery samples of same BPD/DS patients (Figure 33A, 33E).

5.0 DISCUSSION

The mechanisms contributing to gut microbiota-driven changes in obesity and T2D remain unclear. Alterations in gut microbiota can lead to changes in microbiota richness and diversity as well as microbiota's ability to extract energy from food, which together influence energy balance and lipid deposition. Gut microbiota can also influence host sugar transport and satiety-related gut hormone regulation, insulin sensitivity and blood glucose control⁸⁰. The gut microbiota also influences many aspects of immune system development, including innate and adaptive aspects of immunity, gut barrier function and gut permeability^{80,103}. The gut microbiota also generates unique metabolites (such as SCFAs) that have wide-ranging effects on host immunity and metabolism. These immunometabolism factors can work together to alter inflammation, energy balance and blood glucose homeostasis. The purpose of this thesis was to test if alterations in the microbiota induced by bariatric surgery was an independent factor that alters host blood glucose control and then to probe the underlying mechanism of action that could mediate this microbe-host response. We found that GF mice receiving post-surgery FMT from bariatric surgery patients had significantly lower blood glucose comparing to those with pre-surgery FMT from the same patients. This lowering blood glucose effect was due to insulin-independent mechanisms, including alterations in the intestinal glucose absorption. Changes in intestinal morphological characteristics were also associated with better glucose control in GF mice.

5.1 Blood glucose homeostasis was improved in GF mice receiving post-surgery FMT

It was known that bariatric surgery altered gut microbiota composition in human patients and it is associated with better glucose control and T2D remission in a significant number of patients^{22,45,46}. Here we showed that FMT from post-bariatric surgery patients was a stand-alone factor that could improve glucose tolerance in GF mice. We found that exposing GF mice to fecal microbes present ~1 year after surgery lowered blood glucose during an oral glucose challenge when directly compared to GF mice exposed to fecal microbes from the same patients before bariatric surgery. Importantly, GF mice must be exposed to these human microbes for at least 7 weeks in order for changes in glycemia to manifest, an effect that is consistent with our previous results showing that the exposure time to gut microbes is a key factor dictating the effect of the microbiota on obesity-induced changes in blood glucose⁸⁹. We also tested fecal microbes from two different types of bariatric surgery patients and found that both restrictive and malabsorptive types of bariatric surgery promoted changes in the fecal microbiota that improved glucose control. We then focused on BPD/DS, since it was the most potent type of bariatric surgery for improvement in blood glucose. We aimed to understand whether improved glucose homeostasis induced by FMT results from changes in insulin sensitivity, insulin secretion or intestinal glucose transport. We found no differences in insulin or c-peptide levels in the serum of GF mice after FMT from pre- and post-

surgery BPD/DS patients. Therefore, FMT-driven improvement in glucose homeostasis in GF mice was not associated with increased insulin secretion. The HOMA-IR index was next used to estimate insulin resistance in the fasted state of GF mice and we found that FMT from pre- and post-surgery BPD/DS patients did not alter this index of insulin resistance. Thus, we found little evidence of changes in insulin levels or insulin resistance in GF mice after FMT, which leaves microbe-induced changes in glucose absorption as a candidate for changes in glucose homeostasis.

5.2 Changes in the expression of genes involved in intestinal glucose absorption was associated with improved glucose homeostasis in GF mice

We next investigated mechanisms that could underpin changes in glucose absorption. We analyzed expression levels of genes involved in intestinal glucose absorption in GF mice after FMT using fecal samples before and after BPD/DS and VSL. We found decreases in the transcript level of *Glut1* in the ileum of mice receiving post-surgery FMT. Changes in *Glut1* expression can correlate with cellular glucose transport. For example, increased *Glut1* correlated with higher intestinal glucose uptake and improved glycemic control seen in RYGB-treated rats when compared to sham-operated rats²⁶. Higher *Glut1* was also seen in gastrointestinal carcinoma and it acts as a potential marker for malignant transformation⁹⁸. Our study has shown contradictory results that decreased *Glut1* correlated with improved glycemic control in GF mice that received post-surgery fecal microbiota from patients undergone BPD/DS or VSL

bariatric surgery. One explanation may be that GF mice involved in this study did not undergo any surgery or gut segment rearrangement. The effect of FMT alone on glycemia control and intestinal glucose absorption is a subset of the potent effects of bariatric surgery, and thus may not involve changes on the transcript level of genes involved in glucose absorption. More importantly, we followed this mRNA expression analysis by measuring changes in GLUT1 protein in the ileum. We found that FMT did not alter GLUT1 protein levels in the ileum, suggesting that the change in intestinal GLUT1 is not a key mechanism that could explain improved glucose control in GF mice after FMT.

Changes in the transcript level of *Glut1* was not localized to the intestine. GF mice that received FMT from post-surgery BPD/DS donors had significantly lower *Glut1* transcript level in the upper intestine, but also higher *Glut1* transcript level in the hindlimb skeletal muscle. Skeletal muscle contributes to a large portion of total body mass and contributes as a sink for blood glucose disposal⁹⁹. In fact, impaired muscle glucose uptake is associated with decreased GLUT1 protein levels in the skeletal muscle⁹⁸. Therefore, the increased *Glut1* transcript level seen in the TA muscle of GF mice that received FMT from post-surgery BPD/DS donors may be associated with increased glucose disposal during the oGTT conducted in our study. This correlation would fit with the insulin-independent action of GLUT1 (as opposed to insulin-dependent action of GLUT4) since our results showed no changes in blood insulin or whole body indices of insulin sensitivity. Therefore, one possibility is that FMT with post-

surgery microbes leads to higher levels of muscle GLUT1, which promote increased insulin-independent disposal of blood glucose in GF mice. The microbe-induced signals that connect a gut-muscle axis are not yet clear, but there are several candidate molecules and pathways, including SCFAs^{100,101}. These results warrant future investigation of GLUT1 protein levels in skeletal muscle and microbial mediators of a gut-muscle axis.

5.3 Alteration in blood glucose homeostasis was associated with changes in the gut morphology of GF mice

We next investigated how FMT altered features of the intestine other than the expression of glucose transporters. Surprisingly, we found that FMT altered the architecture of the intestine. We demonstrated that the number of goblet cells per 10 crypts was significantly decreased in the duodenum/jejunum and ileum of GF mice with post-surgery FMT from BPD/DS patients. The ileum of GF mice with post-surgery FMT also had lower mean villus height and crypt depth, compared to those that received FMT from the pre-surgery samples of same BPD/DS patients. It is known that crypt depth, villus height and goblet cell number in each intestinal segment are associated with food absorption efficiency and inflammation^{102,103}. In the small intestine, shorter villi and deeper crypts are associated with fewer absorptive and more secretory cells, leading to impaired nutrient absorption¹⁰². In addition, these morphometric characteristics influence the pathogenesis of diarrhea, as demonstrated in postweaning pigs¹⁰². Goblet cells also secrete mucins, which act as the main structural component of

intestinal mucus layer, the frontline of innate host defense against microbial invasion¹⁰⁴⁻¹⁰⁶. An elevated goblet cell count and the development of goblet cell hyperplasia are associated with pathogenic microbial infection¹⁰³. In our study, we found lower goblet cell count and shorter villus height are correlated with better glucose control, which are both observed in GF mice with post-surgery FMT from BPD/DS patients. Nevertheless, whether better glucose control seen in these GF mice accompanies with impaired nutrient absorption and less microbial infection remains unknown.

5.4 Future directions

The results of this thesis have shown that fecal microbes from humans after bariatric surgery are a stand-alone factor that can alter blood glucose, and the intestinal architecture in GF mice exposed to this new microbial community for a sufficient duration (i.e. 7 weeks) can be changed. Our results show changes in goblet cell numbers, but an important future direction will be to assess the progression of alterations in the innate and adaptive immune systems in different tissues of GF mice that received FMT from bariatric surgery patients. An interesting future direction would be to characterize circulating immune factors and cells in tissues that help control blood glucose and the intestine. Other aspects of immunity should also be investigated after FMT. For example, it should be examined whether the mucus thickness and bacterial encroachment towards the epithelial barrier are affected by FMT from patients before and after

bariatric surgery. The mucus layer, comprised of goblet cells, can influence inflammation by providing a barrier between luminal bacteria and the host epithelium¹⁰⁷. Mice with a thinner mucus layer have more contact between the epithelium and luminal bacteria, which leads to exacerbation of a transient inflammatory state around the time of weaning¹⁰⁸. Bacterial encroachment refers to the shrinking of a “bacteria-free” zone that is adjacent to the epithelium¹⁰⁹. Bacterial encroachment is associated with inflammatory bowel disease in human and colitis and metabolic syndrome in mouse models, which can lead to low-grade inflammation^{109,110}. In diabetic human patients, the primary predictor of bacterial encroachment is dysglycemia; however, the same result was not confirmed in mouse models since high glucose levels alone were not able to cause encroachment in mice¹⁰⁹. An important future direction would be to test if human-associated gut bacteria rather can influence hyperglycaemia-induced encroachment in mice. The relationships between mucus layer thickness, bacterial encroachment, glycemia and inflammation warrant further examination.

One aspect that should be examined is small intestinal epithelial cell (IEC) staining, which would allow visualization of structural characteristics of the IECs in the GF mice that received bariatric surgery patient FMT. Conducting fluorescent in situ hybridization (FISH) would then allow visualization of bacteria location, which further allows the quantification of bacterial encroachment in the intestine. Specific probes for different bacteria strains could also be developed to detect if certain bacteria are prone to bacterial encroachment.

We could also assess glucose absorption in the mice by means of glucose analog, such as 3-O-methyl glucose (3-OMG). 3-OMG is absorbed by the same intestinal transport mechanism as glucose. Unlike glucose, it is not metabolized by the liver^{111,112}. Therefore, plasma [3-OMG] can be used as an index of glucose absorption. Dr. Fernando Forato Anê from Schertzer lab has conducted a study with GF mice that received fecal material from BPD/DS donors. He showed that after 7 weeks of FMT, GF mice receiving post-BPD/DS-surgery fecal material has a significantly lower rate of 3-OMG absorption compared to those receiving pre-BPD/DS-surgery fecal material (Figure 34). This reveals that gut microbiota could lead to differences in glucose absorption in GF mice and is worth further investigation.

In addition, it would be beneficial to perform 16S RNA and/or metagenomic sequencing on the intestinal segment-specific microbiome to obtain a bacterial profile from the GF mice that received FMT from BPD/DS or VSL patients. It would be interesting to determine if certain strains of bacteria have altered population in the GF mice that received post-surgery FMT, which correlated with better glucose tolerance. If such bacteria strains are found, we could further test if they are standalone factors to induce improved glucose control in GF mice. This could be tested by transplanting GF mice with these specific strains of bacteria and conduct oGTT tests to measure their blood glucose.

Last but not least, it is possible that FMT of bariatric surgery patients' fecal sample into GF mice does not only lead to changes in the transcript level of genes involved in glucose transport, but also those that are involved in inflammation. qPCR could be performed on tissues and gut segments, with targets such as TNF- α , IL-4, interferon gamma (IFN- γ) among many other factors.

5.5 Limitations

There are several limitations in this thesis. In our model of study, female SPF and GF mice were transplanted with fecal material from female donors that underwent bariatric surgery. The effect of sex should be determined using FMT from male bariatric surgery patients into male SPF and GF mice. Further, it would be interesting to expose female mice to the microbes from male human donors and vice versa. Additionally, it is recognized that fecal material from the human donors is not able to represent the whole microbiota of the donor as it only contains a small subset of the donor's microbes. These studies were limited by the starting material that could be obtained from bariatric surgery patients, which was only fecal material and not from other gut segments. Further, the fecal material from humans had to be frozen and stored before use in GF mice. Freezing the fecal bacterial community can affect the viability of certain bacteria. However, despite this limitation, we found that FMT could alter blood glucose in mice. Hence, an important future test will be to assess if live bacteria are

required to change blood glucose in mice. It is possible that postbiotics and dead bacteria are sufficient to alter blood glucose during the FMT.

Our experiments were also limited by what could be achieved in a limited supply of GF mice and what can be done reliably in a single mouse given ethical and blood volume constraints. As mentioned in the results section, we have calculated HOMA-IR to assess the level of insulin resistance in mice. However, we have not examined the insulin sensitivity of these mice by means of hyperinsulinemic euglycemic clamps, which is often used as a gold standard for directly measuring insulin resistance and can detect tissue-specific glucose disposal.

Finally, our experiments focus on the potential effects of changes in insulin resistance or glucose absorption have on glucose homeostasis in mice. It is not known how changes in the immune system contribute to the blood glucose phenotype observed in GF mice that received post-surgery FMT. As mentioned in the future directions, it will be of our interest to investigate if there are transcriptional or cellular differences in genes that are involved in inflammation.

6.0 CONCLUSION

Bariatric surgery can lead to weight loss and improved glucose tolerance in humans and this surgical intervention alters the composition of intestinal microbiota. However, the mechanism by which gut microbiota alters blood glucose after bariatric surgery is still not well understood. We have completed studies to test the direct effect of changes in microbiota within the same patient before and after two types of bariatric surgery by colonizing mice with the fecal material from human patients. We found that FMT caused no significant changes in body weight, fat mass, glucose tolerance or glucose transporter mRNA expression in all intestine segments in SPF mice that already harbored a complex gut microbiota. However, FMT into GF mice lowers blood glucose during an oral glucose challenge when post-surgery human fecal samples were used after either a restrictive or malabsorptive bariatric surgery. Despite observing a blood glucose lowering effect, we found no evidence for the microbiota-induced changes in blood insulin or insulin sensitivity, which pointed towards FMT's role in altering glucose absorption. There was no consistent signature of changes in intestinal glucose transporters associated with changes in blood glucose caused by post-surgery FMT other than decreased ileal *Glut1* transcript levels, which was not confirmed at the GLUT1 protein level. However, exposure to post-surgery microbes was sufficient to alter intestinal architecture in mice, with a significant decrease in goblet cell count, villus height and crypt depth in the ileum after FMT. Future research should elucidate specific microbial factors that

connect a gut-muscle axis or influence intestinal carbohydrate absorption. This would provide greater insight into mechanisms of how gut microbiota regulates blood glucose and factors that can be targeted to generate new therapies for diabetic patients.

7.0 REFERENCES

1. Kahn SE, Hull RL, Utzschneider KM. 2006. Mechanisms linking obesity to insulin resistance and type 2 diabetes. *Nature* **444**:840–846.
2. DiBaise JK, Zhang H, Crowell MD, Krajmalnik-Brown R, Decker GA, Rittmann BE. 2008. Gut microbiota and its possible relationship with obesity. *Mayo Clin Proc* **83**:460–469.
3. WHO. Fact Sheet - Overweight and obesity. 2018; Available at:<https://www.who.int/en/news-room/fact-sheets/detail/obesity-and-overweight>
4. Lipscombe LL, Hux JE. 2007. Trends in diabetes prevalence, incidence, and mortality in Ontario ,Canada 1995 – 2005 : a population-based study. *The Lancet* **369**:750–756.
5. WHO. Fact Sheet - Diabetes. 2018; Available at <https://www.who.int/news-room/fact-sheets/detail/diabetes>
6. Narayan KMV, Boyle JP, Thompson TJ, Gregg EW, Williamson DF. 2007. Effect of BMI on Lifetime Risk for Diabetes in the U.S. *Diabetes Care* **30** (6): 1562-1566.
7. Colditz GA, Willett WC, Rotnitzky A, Manson JE. 2014. Weight gain as a risk factor for clinical diabetes. *Ann Intern Med* **122**:481–486.
8. Kahn, CR. 1985. The Molecular mechanism of insulin action. 1985. *Ann. Rev. Med* **36**:429-51
9. Kahn BB, Flier JS, Kahn BB, Flier JS. 2000. Obesity and insulin resistance *J Clin Invest* **106**:473–481.
10. Schultze SM, Hemmings BA, Niessen M, Tschopp O. 2012. PI3K/AKT, MAPK and AMPK signalling: Protein kinases in glucose homeostasis. *Expert Rev Mol Med* **14**.
11. Tamemoto H, Kadowaki T, Tobe K, Yagi T, Sakura H, Hayakawa T, Terauchi Y, Ueki K, Kaburagi Y, Satoh S, Sekihara H, Yoshioka S, Horikoshi H, Furuta Y,

- Ikawa Y, Kasuga M, Yazaki Y, Aizawa S. 1994. Insulin resistance and growth retardation in mice lacking insulin receptor substrate-1. *Nature* **372**: 182-186.
12. Withers DJ, Gutierrez JS, Towery H, Burks DJ, Ren J, Previs S, Zhang Y, Bernal D, Pons S, Shulman GI, Bonner-weir S, White MF, Hughes H. 1998. Disruption of IRS-2 causes type 2 diabetes in mice. *Nature* **372**: 900-904.
13. Banerjee S, Saito K, Ait-Goughoulte M, Meyer K, Ray RB, Ray R. 2008. Hepatitis C Virus Core Protein Upregulates Serine Phosphorylation of Insulin Receptor Substrate-1 and Impairs the Downstream Akt/Protein Kinase B Signaling Pathway for Insulin Resistance. *J virol* 2606-2612.
14. Bjorntorp P, Bergman H, Varnauskas E. 1969. Plasma free fatty acid turnover rate in obesity. *Acta med. scand.* 185:351–356.
15. Schinner S, Scherbaum WA, Bornstein SR, Barthel A. 2005. Molecular mechanisms of insulin resistance. *Diabet Med* **51**: 674–682.
16. Lee YH, Giraud J, Davis RJ, White MF. 2003. c-Jun N-terminal kinase (JNK) mediates feedback inhibition of the insulin signaling cascade. *J Biol Chem* **278**: 2896–2902.
17. Hirosumi J, Tuncman G, Chang L, Görgün CZ, Uysal KT, Maeda K, Karin M, Hotamisligil GS. 2002. A central role for JNK in obesity and insulin resistance. *Nature* **420**:333–6.
18. Banerji MA, Lebowitz J, Chaiken RL, Gordon D, Kral JG, Lebovitz HE. 1997. Relationship of visceral adipose tissue and glucose disposal is independent of sex in black NIDDM subjects. *Am J Physiol* **273**: E425–E432.
19. Rabe K, Lehrke M, Parhofer KG, Broedl UC. 2008. Adipokines and Insulin Resistance. *Mol med* **14**:741–751.
20. Goktas Z, Moustaid-moussa N, Shen C, Boylan M, Mo H. 2013. Effects of bariatric surgery on adipokine-induced inflammation and insulin resistance. *Frontiers Endo* 4:1–13.

21. Rull A, Camps J, Alonso-villaverde C, Joven J. 2010. Insulin Resistance, Inflammation, and Obesity: Role of Monocyte Chemoattractant Protein-1 (or CCL2) in the Regulation of Metabolism. *Mediators of Inflammation* **2010**.
22. Rao RS, Yanagisawa R, Kini S. 2012. Insulin resistance and bariatric surgery. *Obesity reviews*. **13**: 316–328.
23. Earnest CP. 2008. Exercise interval training : An improved stimulus for improving the physiology of pre-diabetes. *Med Hypotheses* **71**:752–761.
24. Bashan N, Burdett E, Hundal HS, Klip A. 1992. Regulation of glucose transport and GLUT1 glucose transporter expression by O₂ in muscle cells in culture. *Phys* **262**: C282-C290.
25. Olson AL, Pessin JE. 1996. Structure, function, and regulation of the mammalian facilitative glucose transporter gene family. *Annu. Rev. Nutr* **16**: 235-56.
26. Saeid N Meoli L, Nestoridi E, Gupta NK, Kvas S, Kucharczyk J, Bonab AA, Fischman AJ, Yarmush ML, Stylopoulos N. 2013. Reprogramming of Intestinal Glucose Metabolism and Glycemic Control in Rats After Gastric Bypass. *Science* **341**: 406-410.
27. Douen AG, Ramla T, Rastogi S, Bilan PJ, Cartee GD, Vranic M, Holloszy JO, Klip A. 1990. Exercise Induces Recruitment of the “Insulin-responsive Glucose Transporter”. *J. Biol* **265**:13427–13430.
28. Leung K. [18F]Fluoro-2-deoxy-2-D-glucose. 2004. Molecular Imaging and Contrast Agent Database (MICAD) [Internet]. *Bethesda (MD): National Center for Biotechnology Information (US)*; 2004-2013.
29. Ferber S, BeltrandelRio H, Jonson JH, Noel RJ, Cassidy LE, Clark S, Becker TC, Hughes SD, Newgard CB. 1994. GLUT-2 Gene Transfer into Insulinoma Cells Confers Both Low and High Affinity Glucose-stimulated Insulin Release. *J. Biol.* **269**:11523–11529.

30. Hughes SD, Johnson JH, Quadde C, Newgard CB. 1992. Engineering of glucose-stimulated insulin secretion and biosynthesis in non-islet cells. *Proc. Natl. Acad. Sci.* **89**:688–692.
31. Mace OJ, Morgan EL, Affleck JA, Lister N, Kellett GL. 2007. Calcium absorption by Ca_v1.3 induces terminal web myosin II phosphorylation and apical GLUT2 insertion in rat intestine. *J Physiol.* **2**:605–616.
32. Kellett GL, Brot-laroche E, Mace OJ, Leturque A. 2008. Sugar Absorption in the Intestine: The Role of GLUT2. *Annu. Rev. Nutr* **28**: 35-54.
33. Ganguly A, Mcknight RA, Raychaudhuri S, Shin B, Ma Z, Moley K, Devaskar SU. 2020. Glucose transporter isoform-3 mutations cause early pregnancy loss and fetal growth restriction. *Am J Physiol Endocrinal Metab.* **292**:1241–1255.
34. Simpson IA, Dwyer D, Malide D, Moley KH, Travis A, Vannucci SJ. 2019. The facilitative glucose transporter GLUT3: 20 years of distinction *Am J Physiol Endocrinol Metab* **295**: E242–E253.
35. Rand B, Depaoli AM, Bell GI, Burant CF, Depaoli AM, Bell GI, Burant CF. 1993. Sequence, tissue distribution, and functional characterization of the rat fructose transporter GLUT5. *Am J Physiol*: G1169-76.
36. Burant CF, Takedatll J, Brot- E, Bellstii GI, Davidsons N. 1992. Fructose Transporter in Human Spermatozoa and Small Intestine Is GLUT5*. *J. Biol. Chem* **267**: 14523-14526.
37. Davidson NO, Hausman AML, Ifkovits CA, Buse JB, Gould GW, Burant CF, Bell GI. 1992. Human intestinal glucose transporter expression and localization of GLUT5. *Am J Physiol* **262**: C795-800.
38. Walle D. 2003. The β-D-glucoside and sodium-dependent glucose transporter 1 (SGLT1)-inhibitor phloridzin is transported by both SGLT1 and multidrug resistance-associated proteins 1/2. *Drug Metab Dispos* **31**: 1288-91.
39. Powell DR, Smith M, Greer J, Harris A, Zhao S, Dacosta C, Mseeh F, Shadoan MK, Sands A, Zambrowicz B. 2013. LX4211 Increases Serum

- Glucagon-Like Peptide 1 and Peptide YY Levels by Reducing Sodium/ Glucose Cotransporter 1 (SGLT1) – Mediated Absorption of Intestinal Glucose. *J Pharmacol Exp Ther* **345**: 250–259.
40. Klec C, Ziomek G, Pichler M, Malli R, Graier WF. 2019. Calcium Signaling in β -cell Physiology and Pathology: A Revisit. *Int. J. Mol. Sci* **20**: 6110.
41. Bauer PV, Duca FA, Waise TMZ, Rasmussen BA, Abraham MA, Dranse HJ, Puri A, O'Brien CA, Lam TKT. 2018. Metformin Alters Upper Small Intestinal Microbiota that Impact a Glucose-SGLT1-Sensing Glucoregulatory Pathway Article Metformin Alters Upper Small Intestinal Microbiota that Impact a Glucose-SGLT1-Sensing Glucoregulatory Pathway. *Cell Metab* **27**:101-117.e5.
42. Maida A, Lamont BJ, Cao X, Drucker DJ. 2011. Metformin regulates the incretin receptor axis via a pathway dependent on peroxisome proliferator-activated receptor- α in mice. *Diabetologia* **54**: 339–349.
43. Zambrowicz B, Ding Z, Ogbaa I, Frazier K, Banks P, Turnage A, Freiman J, Smith M, Ruff D, Sands A, Powell D. 2013. Effects of LX4211, a Dual SGLT1/SGLT2 Inhibitor, Plus Sitagliptin on Postprandial Active GLP-1 and Glycemic Control in Type 2 Diabetes. *Diabetes* **62**:273-285.e7.
44. Zambrowicz B, Freiman J, Brown PM, Frazier KS, Turnage A, Bronner J, Ruff D, Shadoan M, Banks P, Mseeh F, Rawlins DB, Goodwin NC, Mabon R, Harrison BA, Wilson A, Sands A. 2012. LX4211, a Dual SGLT1/SGLT2 Inhibitor, Improved Glycemic Control in Patients With Type 2 Diabetes in a Randomized, Placebo-Controlled Trial. *Nature* **485**: 158-169.
45. Beckman LM, Beckman TR, Earthman CP. 2010. Changes in Gastrointestinal Hormones and Leptin after Roux-en-Y Gastric Bypass Procedure: A Review. *J Am Diet Assoc* **110**:571–584.
46. Miras AD, Le Roux CW. 2013. Mechanisms underlying weight loss after bariatric surgery. *Nat. Rev. Gastroenterol. Hepatol* **10**:575-584.

47. U.K. Prospective Diabetes Study Group. 1998. Perspectives in Diabetes U.K. Prospective Diabetes Study 16 Overview of 6 Years' Therapy of Type II Diabetes: A Progressive Disease. *Diabetes* **44**: 1249–1258.
48. Roux CW, Aylwin SJB, Batterham RL, Borg CM, Coyle F, Prasad V, Shurey S, Ghati MA, Patel AG, Bloom SR. 2006. Gut Hormone Profiles Following Bariatric Surgery Favor an Anorectic State, Facilitate Weight Loss, and Improve Metabolic Parameters. *Annals of Surgery* **243**:108–114.
49. Dixon JB, Roux CW, Rubino F, Zimmet P. 2012. Bariatric surgery for type 2 diabetes. *The Lancet* **379**: 2300-11.
50. Rubino F, Marescaux J. 2004. Effect of duodenal-jejunal exclusion in a non-obese animal model of type 2 diabetes: a new perspective for an old disease. *Ann Surg* **239**: 1-11.
51. Cummings DE. 2009. Endocrine mechanism mediating remission of diabetes after gastric bypass surgery. *Int J Obes* **33**: S33-S40.
52. Kenler HA, Brolin RE, Cody RP. 1990. Changes in eating behaviour after horizontal gastropasty and Roux-en-Y gastric bypass. *Am J Clin Nutr* **52**, 87-92.
53. Ernst B, Thurnheer M, Wilms B, Schultes B. 2009. Differential changes in dietary habits after gastric bypass versus gastric banding operations. *Obes Surg* **19**: 274-280.
54. Smith BR, Schauer P, Nguyen NT. 2011. Surgical Approaches to the Treatment of Obesity: Bariatric Surgery. *Med Clin N Am* **95**:1009-1030.
55. Marihart CL, Brunt AR, Geraci AA. 2014. Older adults fighting obesity with bariatric surgery: Benefits, side effects, and outcomes. *Open Medicine*.
56. Marceau P, Ph D, Hould F, Simard S, Sc M, Lebel S, Bourque R. 1998. Biliopancreatic Diversion with Duodenal Switch. *World J. Surg* **22**:947–954.
57. Goldstone AP, Miras AD, Scholtz S, Jackson S, Neff KJ, Pénicaud L, Geoghegan J, Chhina N, Durighel G, Bell JD, Meillon S, Roux CW. 2016. Link

- Between Increased Satiety Gut Hormones and for Obesity . *J Endocrinol Metab* **101**:599–609.
58. Marceau P, Hould FS, Lebel S, Marceau S, Biron S. 2001. Malabsorptive obesity surgery. *Surg Clin North Am* **81**:1113–1127.
59. Topart P, D M, Becouarn G, D M, Ritz P, Ph D. 2013. Weight loss is more sustained after biliopancreatic diversion with duodenal switch than Roux-en-Y gastric bypass in superobese patients. *Surg Obes Relat Dis* **9**:526–530.
60. Buchwald H, Avidor Y, Braunwald E, Jensen MD, Poris W, Fahrenbach K, Schoelles K. 2004. Bariatric Surgery A Systematic Review and Meta-analysis. *JAMA* **292**: 1724-1737.
61. Tilg H, Moschen AR. 2006. Adipocytokines: mediators linking adipose tissue, inflammation and immunity. *Nature Rev* **6**:772–783.
62. Handisurya A, Riedl M, Vila G, Maier C, Clodi M, Prikoszovich T, Ludvik B, Prager G, Luger A, Kautzky-willer A. 2010. Serum Vaspin Concentrations in Relation to Insulin Sensitivity Following RYGB-Induced Weight Loss. *Obes Surg* **20**: 198–203.
63. Chang HM, Lee HJ, Park HS, Kang JH, Kim KS, Song YS, Jang YJ. 2009. Effects of Weight Reduction on Serum Vaspin Concentrations in Obese Subjects : Modification by Insulin Resistance. *Obesity* **18**: 2105–2110.
64. Golpaie A, Tajik N, Masoudkabar F, Karbaschian Z, Talebpour M, Hoseini M, Hosseinzadeh-attar MJ. 2011. Short-term effect of weight loss through restrictive bariatric surgery on serum levels of vaspin in morbidly obese subjects. *Eur. Cytokine Netw* **22**:181–186.
65. Lu H, Wamba PCF, Lapointe M, Poirler P, Martin J, Bastien M, Clanflone K. 2014. Increased Vaspin Levels Are Associated with Beneficial Metabolic Outcome Pre- and Post-Bariatric Surgery. *PLOS ONE* **9**: e111002.
66. Le Roux CW, Welbourn R, Werling M, Osborne A, Kokkinos A, Laurenus A, Lönroth H, Fändriks L, Ghatei MA, Bloom SR, Olbers T. 2007. Gut hormones

- as mediators of appetite and weight loss after Roux-en-Y gastric bypass. *Ann Surg* **246**:780–785.
67. Adrian TE, Savage AP, Fuessl HS, Wolfe K, Besterman HS, Bloom SR. 1987. Release of peptide YY (PYY) after resection of small bowel, colon, or pancreas in man. *Surgery* **101**: 715-19.
68. Adrian TE, Savage AP, Wolfe K, Besterman HS. 1986. Peptide YY Abnormalities in Gastrointestinal Diseases. *Gastroenterology* **90**: 379–384.
69. Cani PD, Delzenne NM. 2007. Gut microflora as a target for energy and metabolic homeostasis. *Curr Opin Clin Nutr Metab Care* **10**:729–734.
70. Zhang H, DiBaise JK, Zuccolo A, Kudrna D, Braidotti M, Yu Y, Parameswaran P, Crowell MD, Wing R, Rittmann BE, Krajmalnik-Brown R. 2009. Human gut microbiota in obesity and after gastric bypass. *Proc Natl Acad Sci* **106**:2365–2370.
71. Furet JP, Kong LC, Tap J, Poitou C, Basdevant A, Bouillot JL, Mariat D, Corthier G, Doré J, Henegar C, Rizkalla S, Clément K. 2010. Differential adaptation of human gut microbiota to bariatric surgery-induced weight loss: links with metabolic and low-grade inflammation markers. *Diabetes* **59**: 3049-57.
72. Cummings S, Pratt J. 2015. Metabolic and bariatric surgery Nutrition and dental considerations. *J Am Dent Assoc* **146**:767–772.
73. Tremaroli V, Karlsson F, Werling M, Ståhlman M, Kovatcheva-Datchary P, Olbers T, Fändriks L, Le Roux CW, Nielsen J, Bäckhed F. 2015. Roux-en-Y Gastric Bypass and Vertical Banded Gastroplasty Induce Long-Term Changes on the Human Gut Microbiome Contributing to Fat Mass Regulation. *Cell Metab* **22**:228–238.
74. Turnbaugh PJ, Ley RE, Mahowald MA, Magrini V, Mardis ER, Gordon JI. 2006. An obesity-associated gut microbiome with increased capacity for energy harvest. *Nature* **444**:1027–1031.

75. Turnbaugh PJ, Hamady M, Yatsunencko T, Cantarel BL, Ley RE, Sogin ML, Jones WJ, Roe BA, Jason P, Egholm M, Henrissat B, Heath AC, Knight R, Gordon JI. 2009. A core gut microbiome in obese and lean twins. *Nature* **457**:480–484.
76. Kalliomäki M, Collado MC, Salminen S, Isolauri E. 2008. Early differences in fecal microbiota composition in children may predict overweight. *Am J Clin Nutr* **87**: 534–538.
77. Ley RE, Turnbaugh PJ, Klein S, Gordon JI. 2006. Human gut microbes associated with obesity. *Nature* **444**: 1022–1023.
78. Fei N, Zhao L. 2013. An opportunistic pathogen isolated from the gut of an obese human causes obesity in germfree mice. *ISME J* **7**: 880–884.
79. Sepp E, Kolk H, Lõivukene K, Mikelsaar M. 2014. Higher blood glucose level associated with body mass index and gut microbiota in elderly people. *Microbial Ecology in Health and Disease* **25**:22857.
80. Caricilli AM, Saad MJA. 2013. The Role of Gut Microbiota on Insulin Resistance. *Nutrients* **5**: 829–851.
81. Sotos M, Nadal I, Marti A, Martínez A, Matillas MM, Campoy C, Puertollano MA, Wärnberg J, Marcos A, Sanz Y. 2020. Gut microbes and obesity in adolescents. *OCE1* **67**: E20.
82. Santacruz A, Marcos A, Warnberg J, Marti A, Martin-Matillas M, Campoy C, Moreno LA, Veiga O, Redondo-Figuero C, Garagorri JM, Azcona C, Delgado M, Garcia-Fuentes M, Collado MC, Sanz Y. 2009. Interplay between weight loss and gut microbiota composition in overweight adolescents. *Obesity (Silver Spring)* **17** (10), 1906–1915.
83. Seeley RJ, Chambers AP, Sandoval DA. 2015. The Role of Gut Adaptation in the Potent Effects of Multiple Bariatric Surgeries on Obesity and Diabetes. *Cell Metab* **21**:369–378.
84. Murphy R, Tsai P, Jüllig M, Liu A, Plank L, Booth M. 2017. Differential Changes in Gut Microbiota After Gastric Bypass and Sleeve Gastrectomy

- Bariatric Surgery Vary According to Diabetes Remission. *Obes Surg* **27**: 917–925.
85. Bäckhed F, Ding H, Wang T, Hooper L, Koh GY, Nagy A, Semenkovich CF, Gordon JI. 2004. The gut microbiota as an environmental factor that regulates fat storage. *PNAS* **101**: 15718-15723.
86. Matsuzaki T, Yamazaki R, Hashimoto S, Yokokura T. 1997. Antidiabetic effects of an oral administration of *Lactobacillus casei* in a non-insulin-dependent diabetes mellitus (NIDDM) model using KK-Ay mice. *Endocr J* **44**: 357–365.
87. Delzenne NM, Neyrinck AM, Bäckhed F, Cani PD. 2011. Targeting gut microbiota in obesity. *Nat. Rev. Endocrinol* **7**:639–646.
88. Denou E, Lolmède K, Garidou L, Pomie C, Chabo C, Lau TC, Fullerton MD, Nigro G, Zakaroff-girard A, Luche E, Garret C, Serino M, Amar J, Courtney M, Cavallari JF, Henriksbo BD, Barra NG, Foley KP, Mcphee JB, Duggan BM, Neill HMO, Lee AJ, Sansonetti P, Ashkar AA, Khan WI, Surette MG, Bouloumié A, Steinberg GR, Burcelin R, Schertzer JD. 2015. Defective NOD 2 peptidoglycan sensing promotes diet-induced inflammation, dysbiosis, and insulin resistance. *EMBO Mol Med* **7**:259–274.
89. Foley KP, Zlitni S, Denou E, Duggan BM, Chan RW, Stearns JC, Schertzer JD. 2015. Long term but not short term exposure to obesity related microbiota promotes host insulin resistance. *Nat Comm* **9**: 1–15.
90. Garrett WS, Gordon JI, Glimcher LH. 2010. Homeostasis and Inflammation in the Intestine. *Cell* **140**:859–870.
91. Barcelo A, Claustre J, Moro F, Chayvialle JA, Cuber JC, Plaisancié P. 2000. Mucin secretion is modulated by luminal factors in the isolated vascularly perfused rat colon. *Gut* **46**: 218–224.
92. Saad MJA, Santos A, Prada PO. 2020. Linking Gut Microbiota and Inflammation to Obesity and Insulin Resistance. *Physio* **31**: 283–293.
93. Qin J, Li Y, Cai Z, Li S, Zhu J, Zhang F, Liang S, Zhang W, Guan Y, Shen D, Peng Y, Zhang D, Jie Z, Wu W, Qin Y, Xue W, Li J, Han L, Lu D, Wu P, Dai Y,

- Sun X, Li Z, Tang A, Zhong S, Li X, Chen W, Xu R, Wang M, Feng Q, Gong M, Yu J, Zhang Y, Zhang M, Hansen T, Sanchez G, Raes J, Falony G, Okuda S, Almeida M, LeChatelier E, Renault P, Pons N, Batto JM, Zhang Z, Chen H, Yang R, Zheng W, Li S, Yang H, Wang J, Ehrlich SD, Nielsen R, Pedersen O, Kristiansen K, Wang J. 2012. A metagenome-wide association study of gut microbiota in type 2 diabetes. *Nature* **490**:55–60.
94. Besten G Den, Eunen K Van, Groen AK, Venema K, Reijngoud D, Bakker BM. 2013. The role of short-chain fatty acids in the interplay between diet, gut microbiota, and host energy metabolism. *J Lipid Res* **54**:2325–2340.
95. Perry RJ, Peng L, Barry NA, Cline GW, Zhang D, Cardone RL, Petersen KF, Kibbey RG, Goodman AL. 2016. Acetate mediates a microbiome-brain- β cell axis promoting metabolic syndrome. *Nature* **534**:213–217.
96. Foley KP, Zlitni S, Duggan BM, Barra NG, Anhê, Cavallari JF, Henriksbo BD, Chen CY, Huang M, Lau T, Schertzer JD. 2020. Gut microbiota regulates insulin clearance in obese mice. Manuscript submitted for publication.
97. Recombinant Anti-Glucose Transporter GLUT1 antibody [EPR3915] (ab115730). Available at <https://www.abcam.com/glucose-transporter-glut1-antibody-epr3915-ab115730.html?productWallTab=ShowAll>
98. Rathan A, Weiser KR, Pritsker A, Itzkowitz SH, Bodian C, Slater G, Weiss A, Burstein DE. 1998. GLUT1 Glucose Transporter Expression in Colorectal Carcinoma A Marker for Poor Prognosis. *ACS* **83**:34–40.
99. Ciaraldi TP, Mudaliar S, Henry RR. 1995. Glucose transport in cultured human skeletal muscle cells. Regulation by insulin and glucose in nondiabetic and non-insulin-dependent diabetes mellitus subjects. *J Clin Invest* **96**: 2820-27.
100. Lustgarten MS. 2019. The Role of the Gut Microbiome on Skeletal Muscle Mass and Physical Function : 2019 Update. *Frontier in Physiology* **10**:1–4.

101. Frampton J, Murphy KG, Frost G, Chambers ES. 2020. Short-chain fatty acids as potential regulators of skeletal muscle metabolism and function. *Nat Metab.*
102. Nabuurs MJA, Hoogendoorn A. 1993. Villus height and crypt depth in weaned and unweaned pigs, reared under various circumstances in the Netherlands. *Res. Vet. Sci.* **55**: 78–84.
103. Kim JJ, Khan WI. 2013. Goblet Cells and Mucins: Role in Innate Defense Enteric Infections. *Pathogens* **2**: 55–70.
104. Specian RD, Oliver MG. 1991. Functional biology of intestinal goblet cells. *J physio* **260**: 83–93.
105. Kandori H, Hirayama K, Takeda M, Doi K. 1996. Histochemical, Lectin-Histochemical and Morphometrical Characteristics of Intestinal Goblet Cells of Germfree and Conventional Mice. *Exp. Anim* **45**: 155-160.
106. Miller HRP. 1987. Gastrointestinal mucus, a medium for survival and for elimination of parasitic nematodes and protozoa. *Parasitology* **94**: S77-S100.
107. Johansson ME V, Larsson JMH, Hansson GC. 2011. The two mucus layers of colon are organized by the MUC2 mucin, whereas the outer layer is a legislator of host – microbial interactions. *PNAS* **108**:4659–4665.
108. Sovran B, Lu P, Loonen LMP, Hugenholtz F, Belzer C, Stolte EH, Boekschoten M V, Baarlen P Van, Smidt H, Kleerebezem M, Vos P De, Renes IB, Wells JM, Dekker J. 2016. Identification of Commensal Species Positively Correlated with Early Stress Responses to a Compromised Mucus Barrier. *Inflamm Bowel Dis* **22**:826–840.
109. Frey MR. 2017. Bacterial Encroachment in Metabolic Syndrome Too Much Togetherness? *CMPG* **4**: 324–325.
110. Chassaing B, Ley RE, Gewirtz AT. 2014. Intestinal Epithelial Cell Toll-like Receptor 5 Regulates the Intestinal Microbiota to Prevent Low-Grade Inflammation and Metabolic Syndrome in Mice. *Gastroenterology* **147**: 1363-1377.

111. Schwartz MP, Samsom M, Renooij W, Van Steenderen LW, Benninga MA, Van Geenen EJM, Van Herwaarden MA, De Smet MBM, Smout AJPM. 2002. Small bowel motility affects glucose absorption in a healthy man. *Diabetes care* **25**: 1857-61.
112. Fordtran JS, Clodi PH, Soergel KH, Ingelfinger FJ. 1962. Sugar Absorption Tests, with Special Reference to 3-O-Methyl-d-Glucose and d-Xylose. *Annals of Internal Medicine* **57**: 883–891.

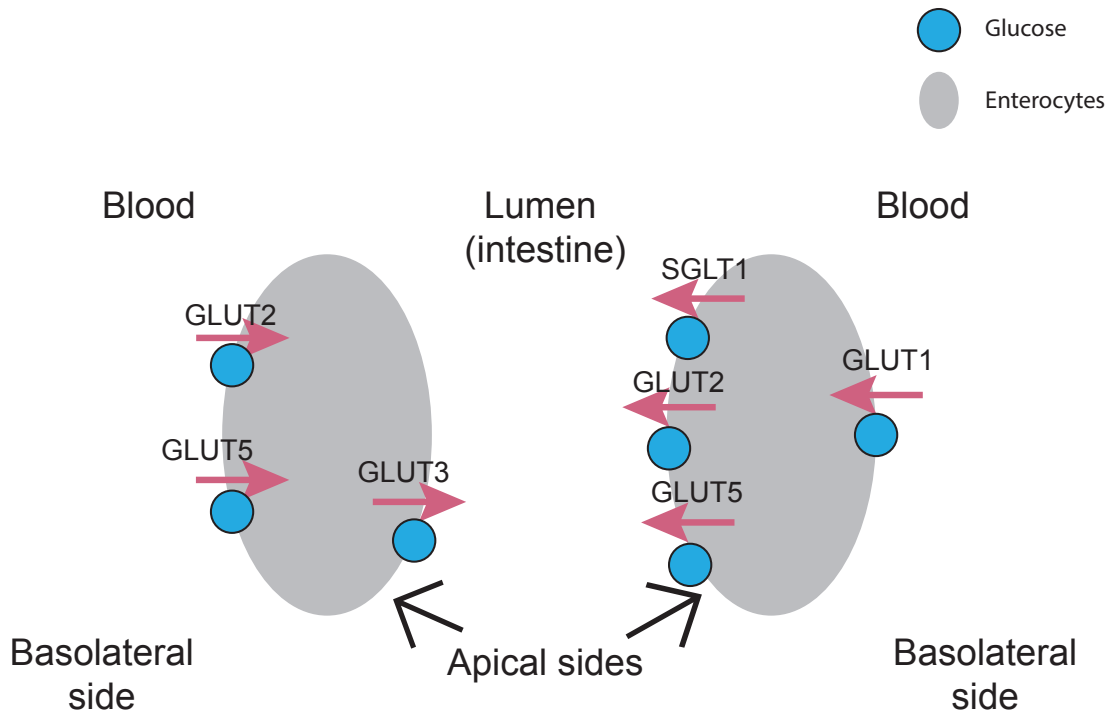


Figure 1: Predominant locations of glucose transporters in the intestine area.

Predominant locations of GLUT1, GLUT2, GLUT3, GLUT5 and SGLT1 depicted in the intestine area.

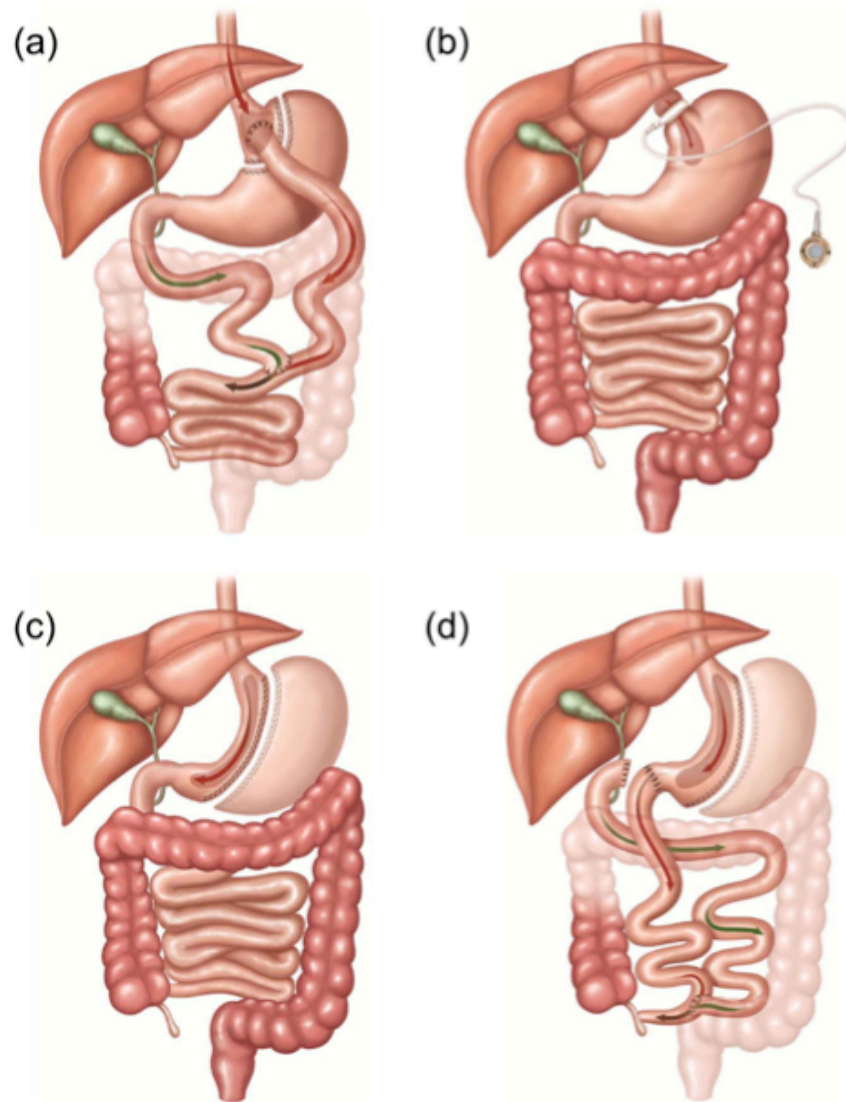


Figure 2: Common types of bariatric surgery.

(a): Roux-en-Y gastric bypass (RYGB); (b): laparoscopic adjustable banding; (c): vertical sleeve gastrectomy (VSL); (d) biliopancreatic diversion with duodenal switch (BPD/DS). All the figures are adapted from *Geraci et al* (2014).

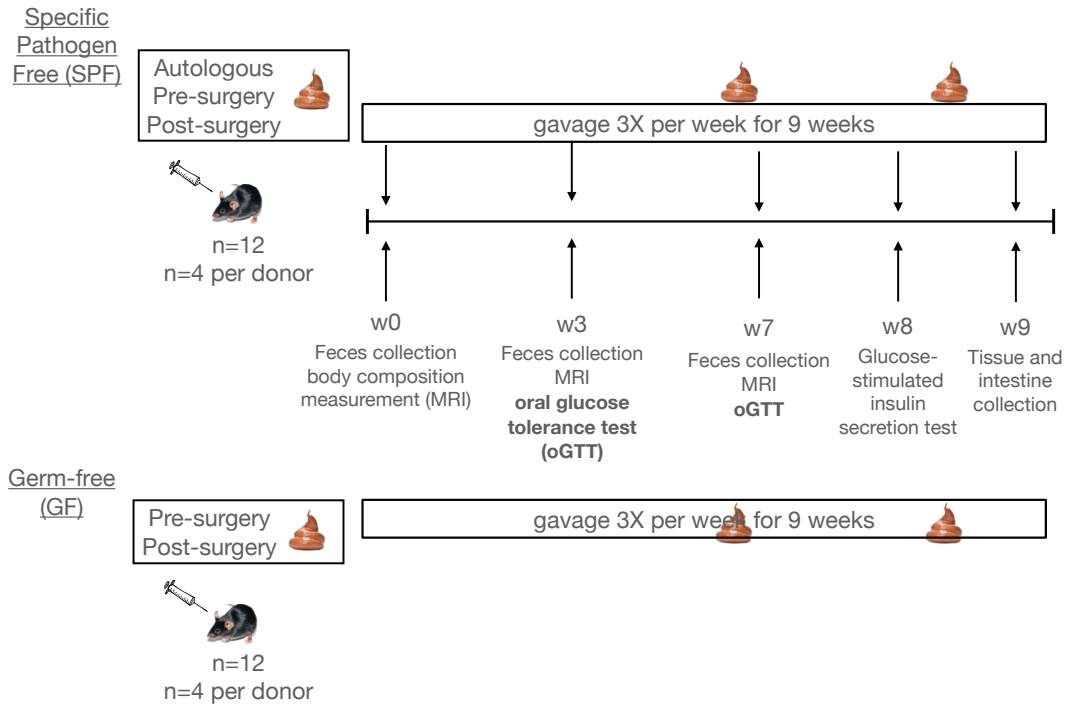


Figure 3: Schematic of experimental design and methods.

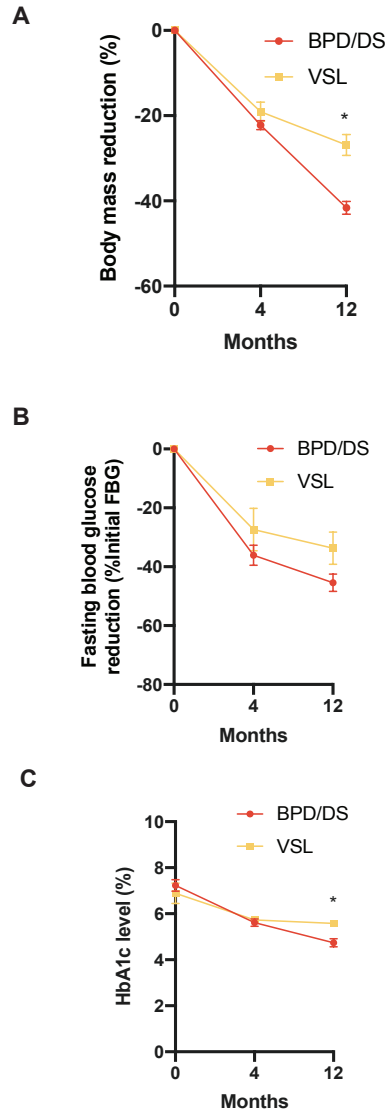


Figure 4: Body mass and blood glucose in bariatric surgery patients

Changes in body mass (**A**), fasting blood glucose (FBG) (**B**), and HbA1c level (**C**) of 12 patients undergone biliopancreatic diversion with duodenal switch (BPD/DS) and 10 patients undergone vertical sleeve gastrectomy (VSL) were recorded at 0, 4 and 12 months after bariatric surgery operation. Values represented as mean \pm SEM, $n=10$ for BPD/DS group and $n=8$ for VSL group. Significant differences between 0 vs 4, 4 vs 12 and 0 vs 12 months are found in patient's BW, FBG and HbA1c level using Tukey's multiple comparison test. *significantly different from the BPD/DS group by multiple t tests.

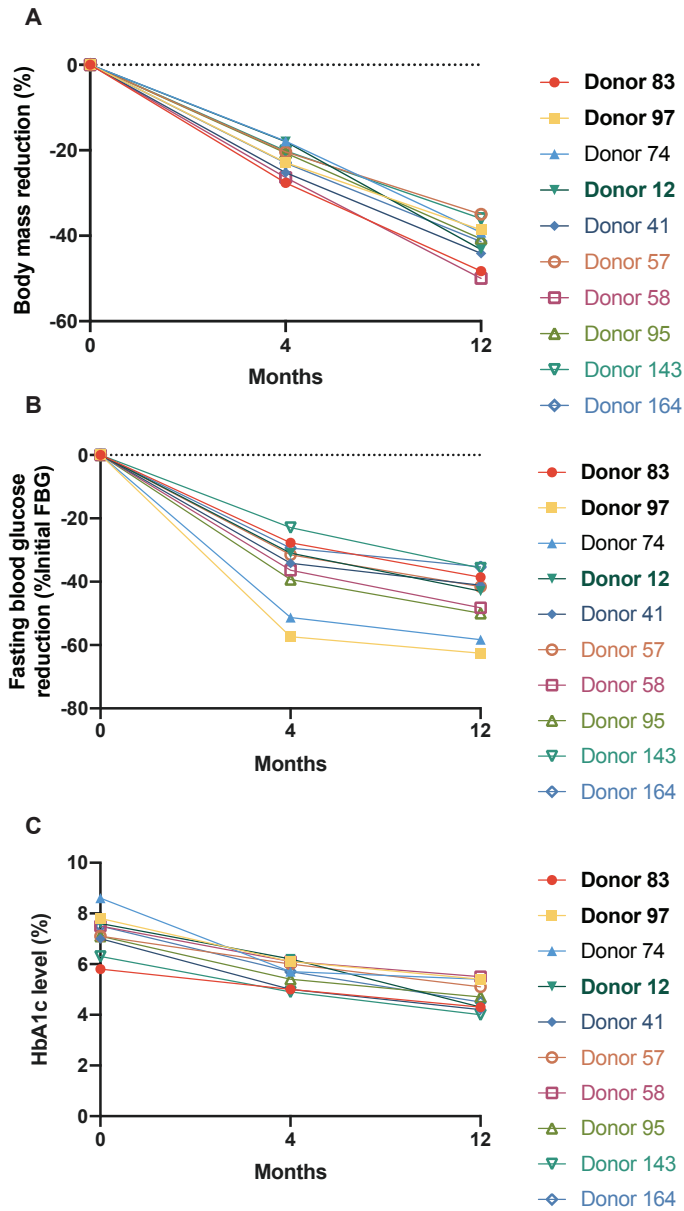


Figure 5: Body mass and blood glucose in BPD/DS surgery patients.

Changes in ten patients' body mass (A), fasting blood glucose (FBG) (B) and HbA1c level (C) were recorded at 0, 4 and 12 months after bariatric surgery operation.

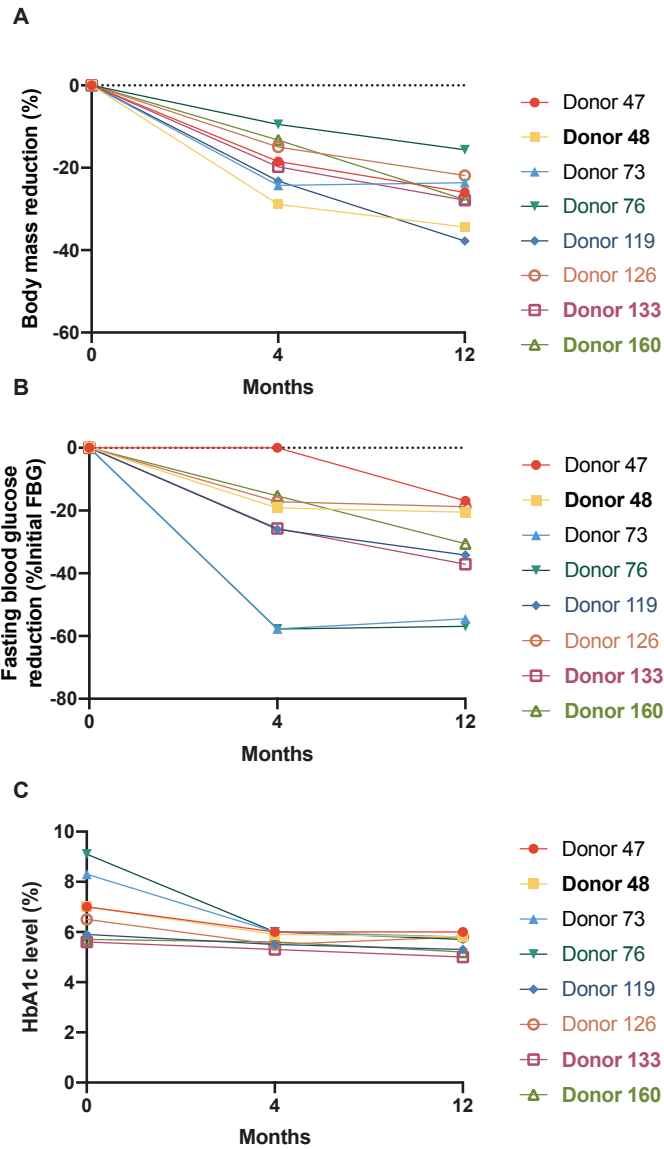


Figure 6: Body mass and blood glucose in VSL surgery patients.

Changes in eight patients' body mass (A), fasting blood glucose (FBG) (B) and HbA1c level (C) were recorded at 0, 4 and 12 months after bariatric surgery operation.

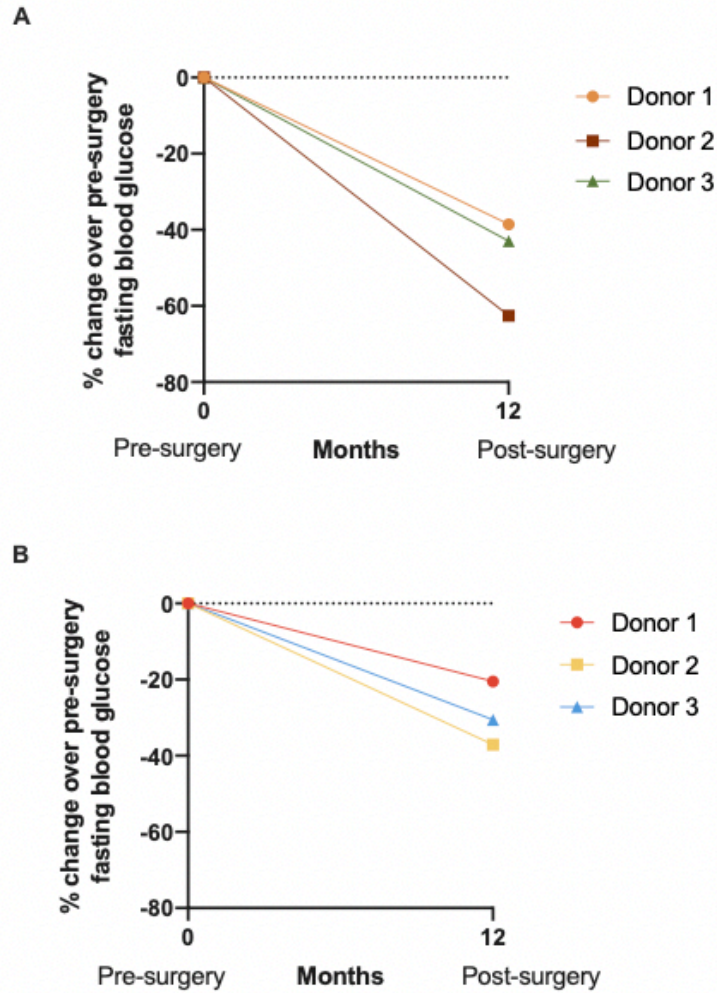


Figure 7: Changes in fasting blood glucose of selected patients undergone bariatric surgeries.

Three patients labeled as Donor 1, Donor 2 and Donor 3 were selected as fecal microbiota donors from the ten BPD/DS patients recorded in Figure 5 (B). Three patients labeled as Donor 1, Donor 2 and Donor 3 were selected as fecal microbiota donors from the eight VSL patients recorded in Figure 6 (B). Percentage change in fasting blood glucose from Pre-surgery to 12 months Post-surgery was recorded for the selected donors.

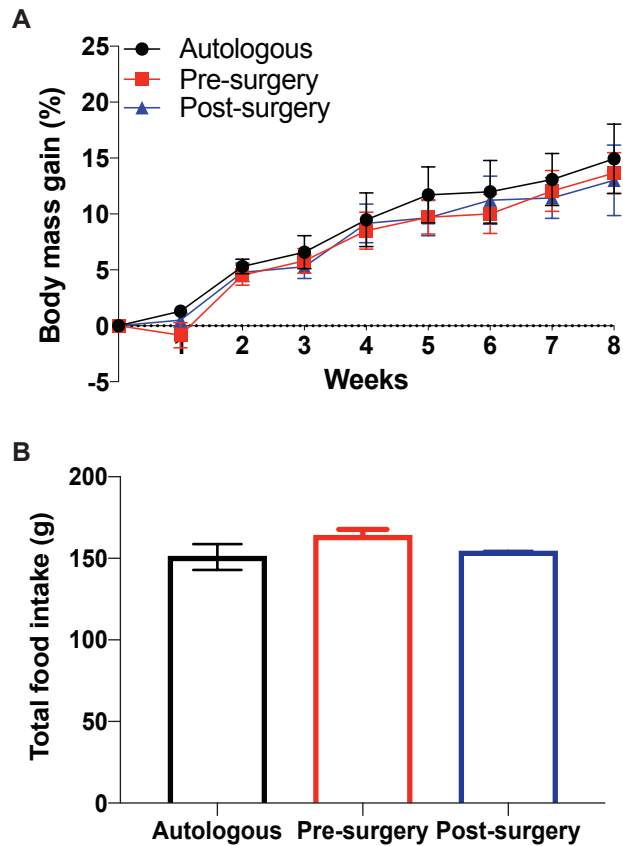


Figure 8: Body features of female SPF mice received fecal microbiota from BPD/DS donors.

Body mass % gain with comparison to base level at week 0 (**A**) and cumulative food intake (**B**) was recorded weekly. Values represented as mean \pm SEM, n=12 for all groups.

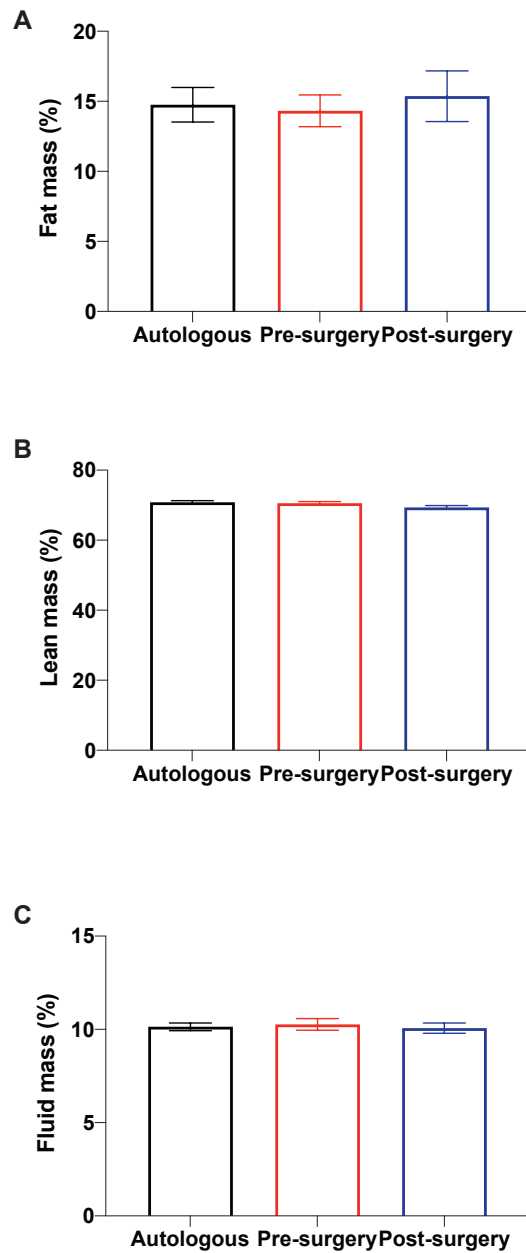


Figure 9: Body composition of female SPF mice received fecal microbiota from BPD/DS donors.

Fat (A), lean (B) and fluid (C) mass were measured at week 7 of the study. Values represented as mean \pm SEM, n=12 for all groups.

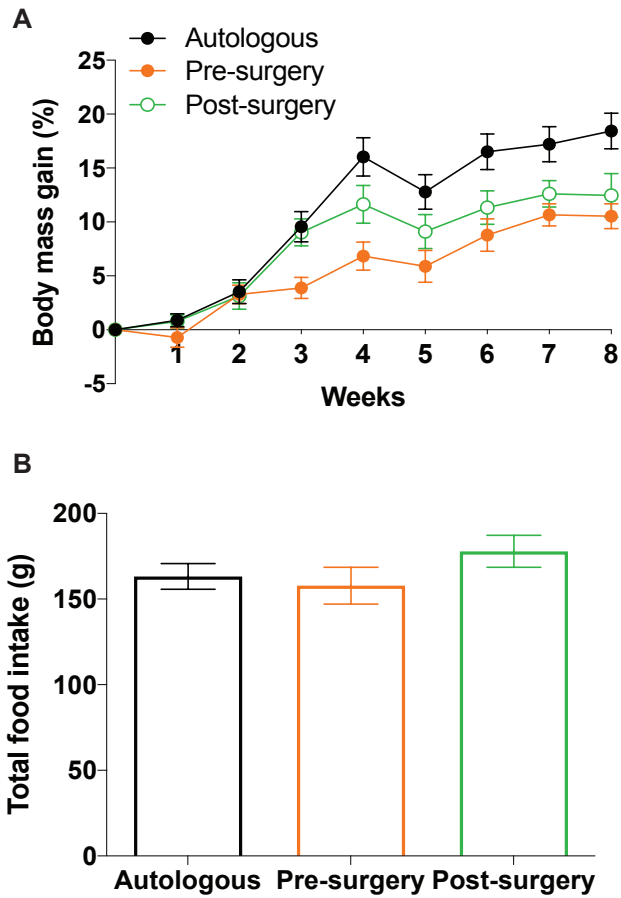


Figure 10: Body features of female SPF mice received fecal microbiota from VSL donors.

Body mass % gain with comparison to base level at week 0 (**A**) and cumulative food intake (**B**) were recorded weekly. Values represented as \pm SEM, $n=12$ for all groups.

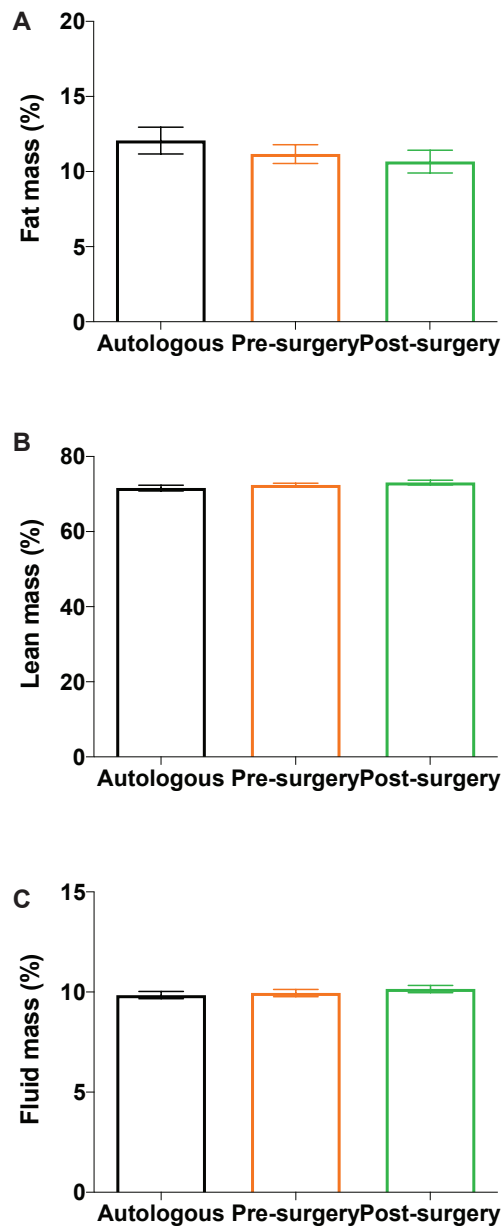


Figure 11: Body composition of female SPF mice received fecal microbiota from VSL donors.

Fat (A), lean (B) and fluid (C) mass were measured at week 7 of the study. Values represented as mean \pm SEM, n=12 for all groups.

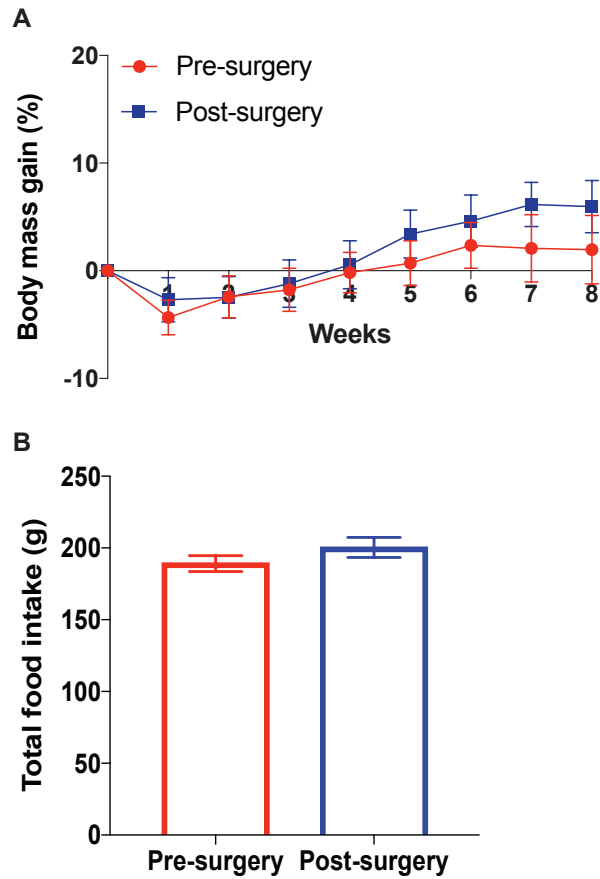


Figure 12: Body features of female GF mice received fecal microbiota from BPD/DS donors.

Body mass % gain with comparison to base level at week 0 (**A**) and cumulative food intake (**B**) were recorded weekly. Values represented as mean \pm SEM, n=11 for Pre-surgery group and n=12 for Post-surgery group.

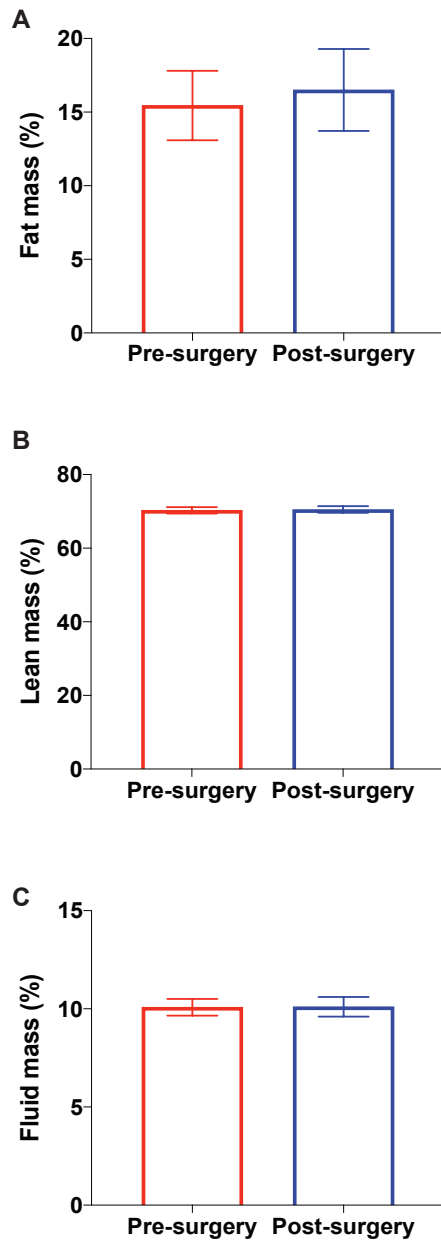


Figure 13: Body composition of female GF mice received fecal microbiota from BPD/DS donors.

Fat (A), lean (B) and fluid (C) mass was measured at week 7 of the study. Values represented as mean \pm SEM, n=11 for Pre-surgery group and n=12 for Post-surgery group.

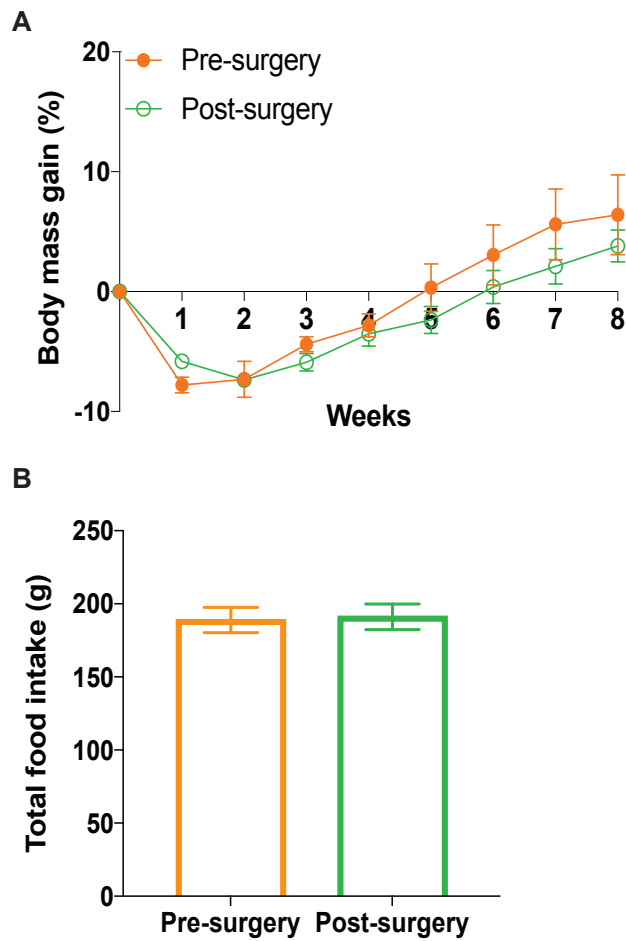


Figure 14: Body features of female GF mice received fecal microbiota from VSL donors.

Body mass % gain with comparison to base level at week 0 (A) and cumulative food intake (B) were recorded weekly. Values represented as mean \pm SEM, n=10 for both groups.

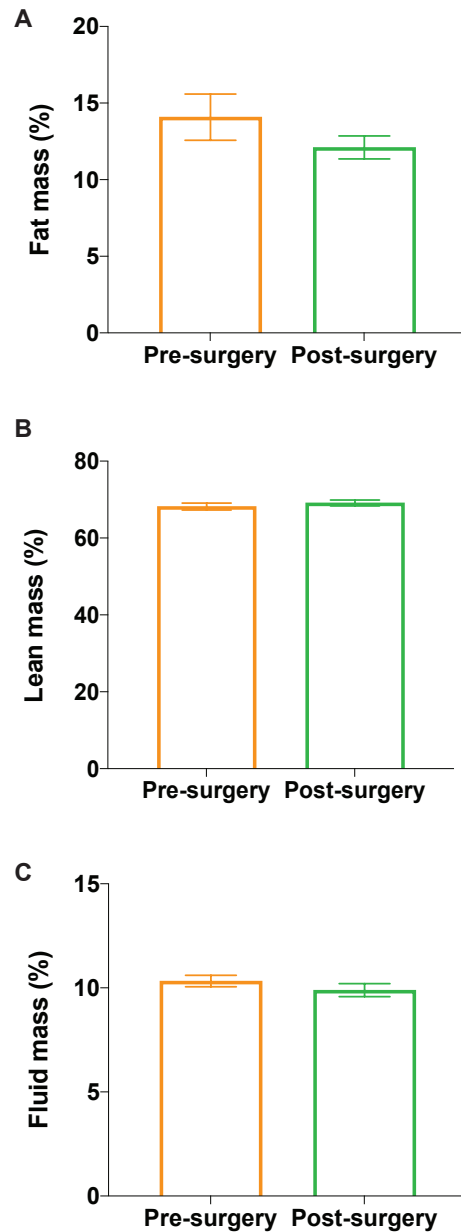


Figure 15: Body composition of female GF mice received fecal microbiota from VSL donors.

Fat (A), lean (B) and fluid (C) mass were measured at week 7 of the study. Values represented as mean \pm SEM, n=10 for both groups.

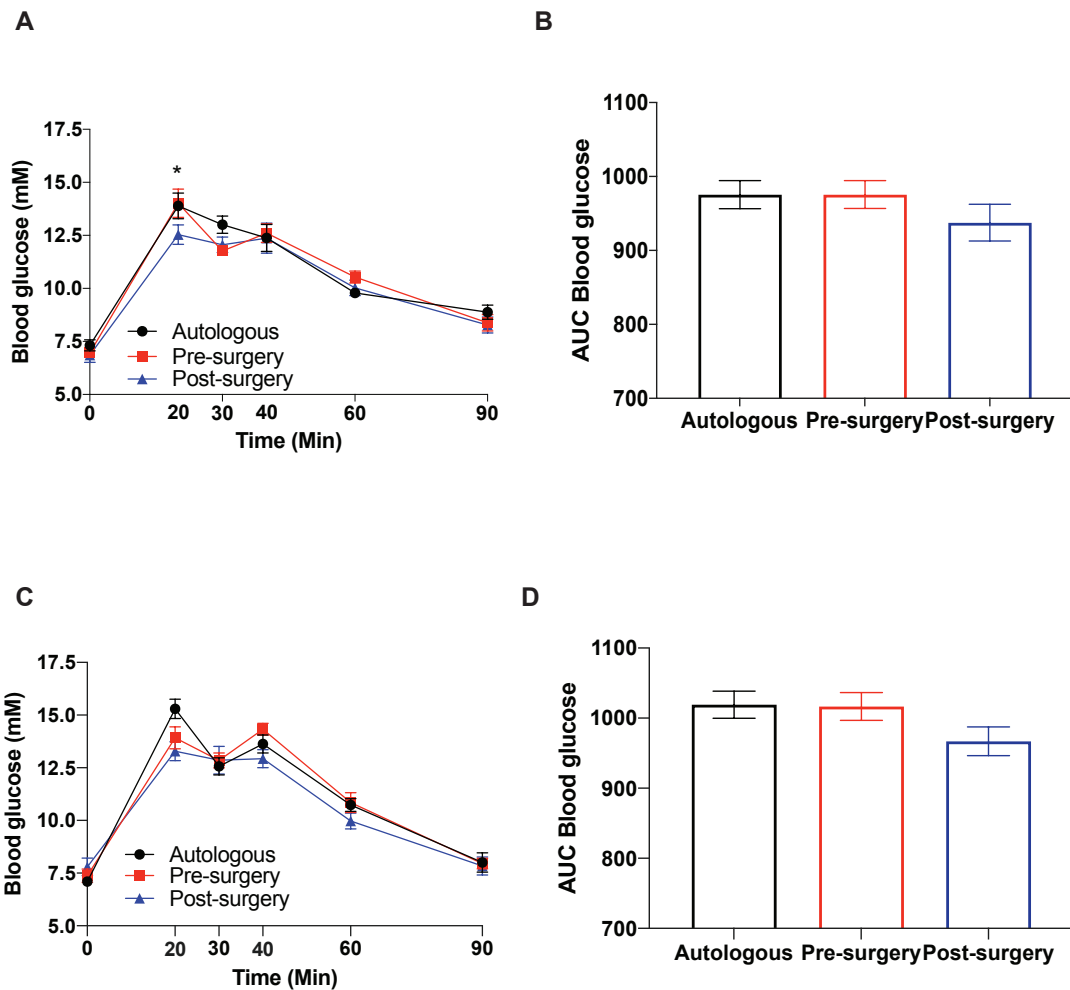


Figure 16: Glucose curve and corresponding AUC in female SPF mice received fecal microbiota from BPD/DS donors.

Glucose curve and corresponding AUC recorded at week 3 (**A and B**) and week 7 (**C and D**) of the study. Values are mean \pm SEM, n=12 for all groups, *significantly different between the pre and post-surgery groups by two-way ANOVA.

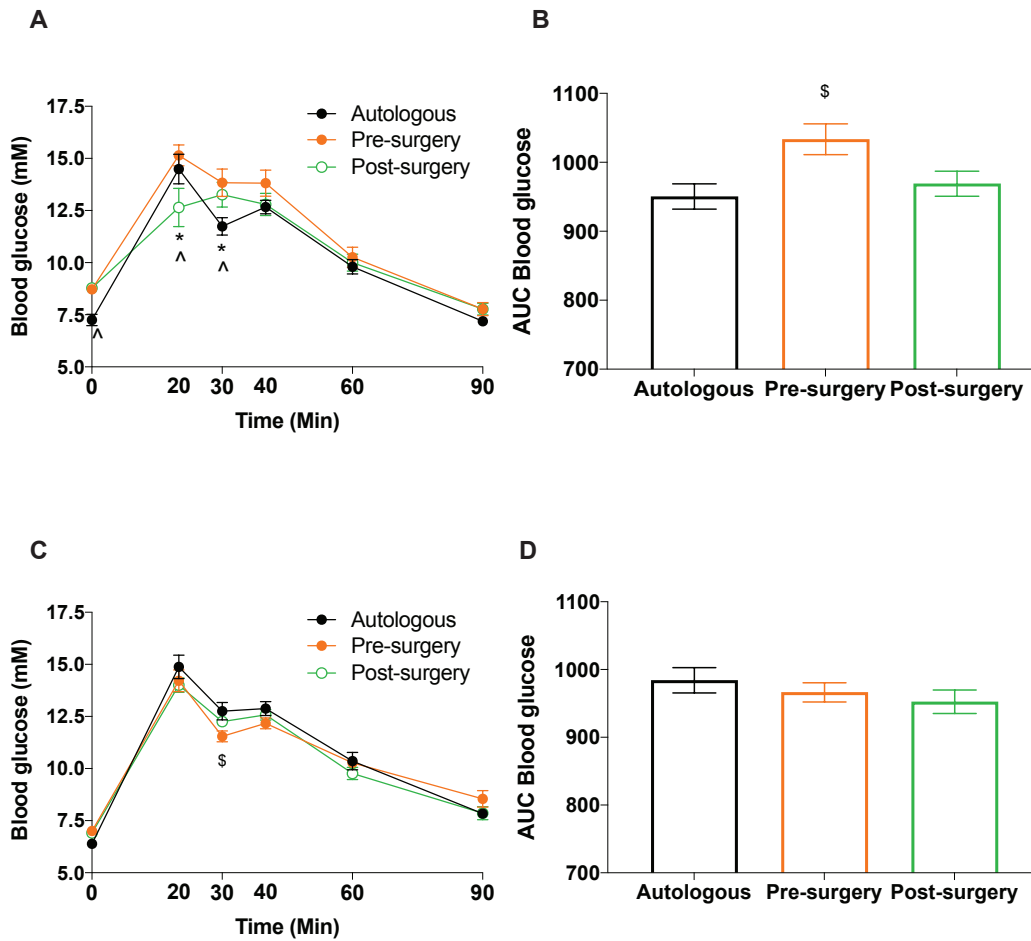


Figure 17: Glucose curve and corresponding AUC in female SPF mice received fecal microbiota from VSL donors.

Glucose curve and corresponding AUC recorded at week 3 (**A and B**) and week 7 (**C and D**) of the study. Values are mean \pm SEM, n=12 for all groups, *significantly different between the pre and post-surgery groups, ^significantly different between autologous and post-surgery groups, \$significantly different between autologous and pre-surgery groups by two-way ANOVA.

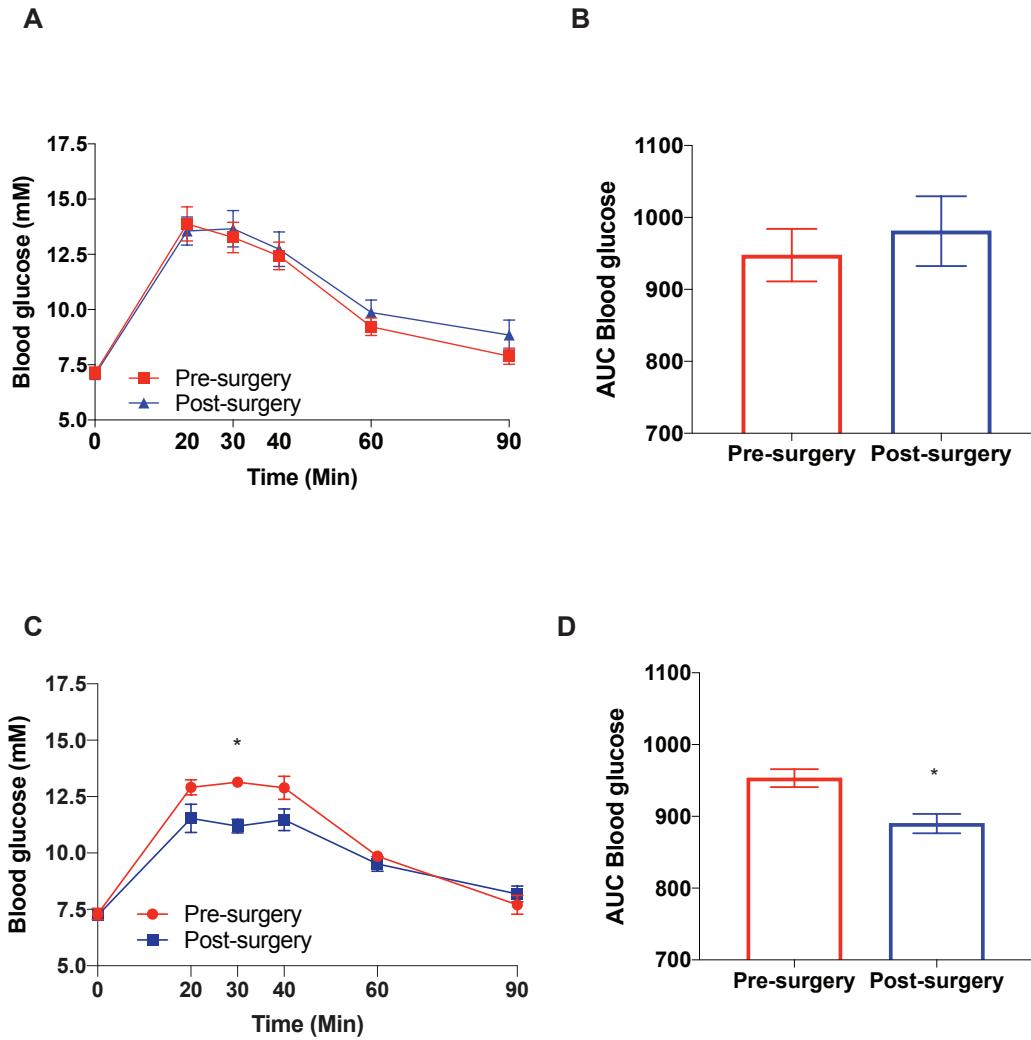


Figure 18: Glucose curve and corresponding AUC in female GF mice received fecal microbiota from BPD/DS donors.

Glucose curve and corresponding AUC recorded at week 3 (**A and B**) and week 7 (**C and D**) of the study. Values are mean \pm SEM, n=11 for Pre-surgery group and n=12 for Post-surgery group. *significantly different from pre-surgery group by Mann-Whitney test.

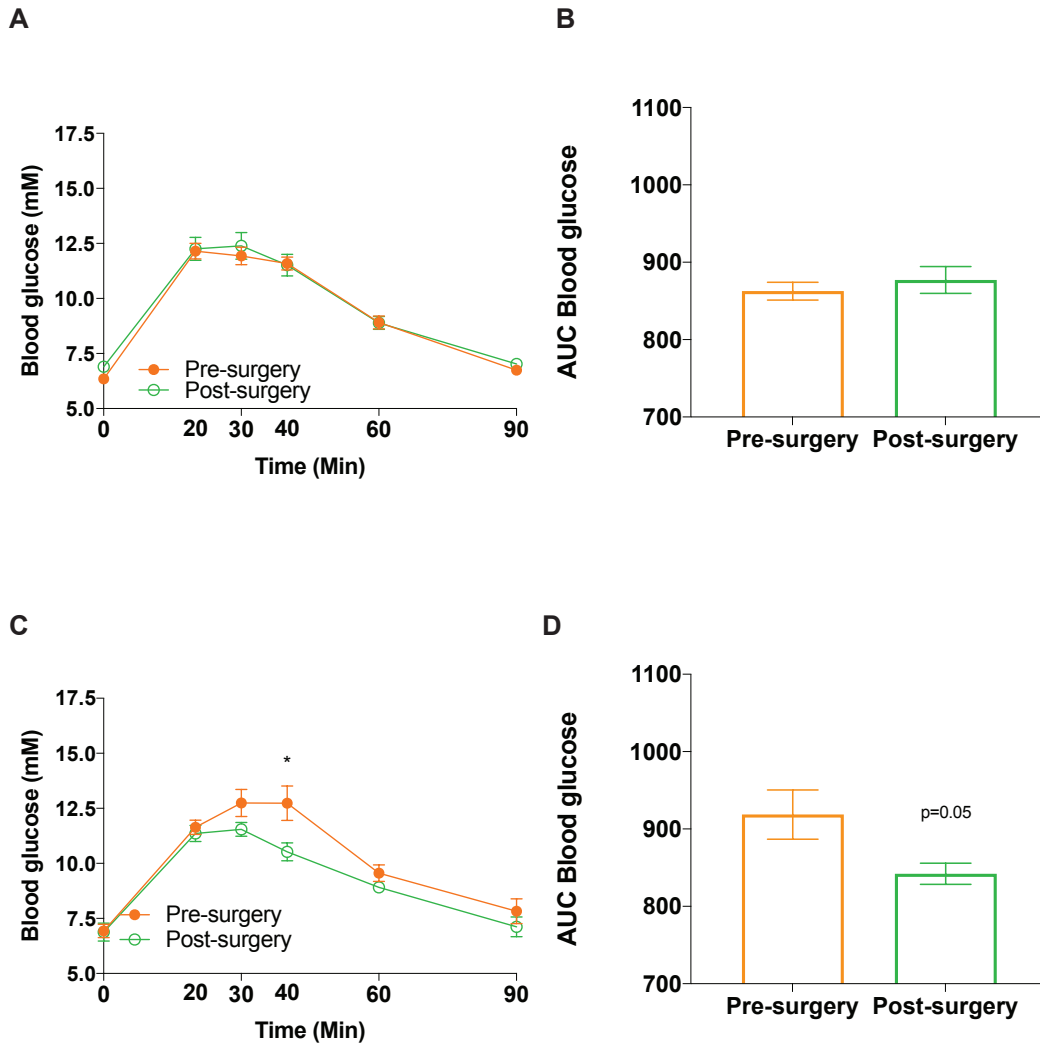


Figure 19: Glucose curve and corresponding AUC in female GF mice received fecal microbiota from VSL donors.

Glucose curve and corresponding AUC recorded at week 3 (**A and B**) and week 7 (**C and D**) of the study. Values are mean \pm SEM, $n=10$ for both groups, *significantly different from pre-surgery group by Mann-Whitney test. $p=0.05$ for **Figure D**.

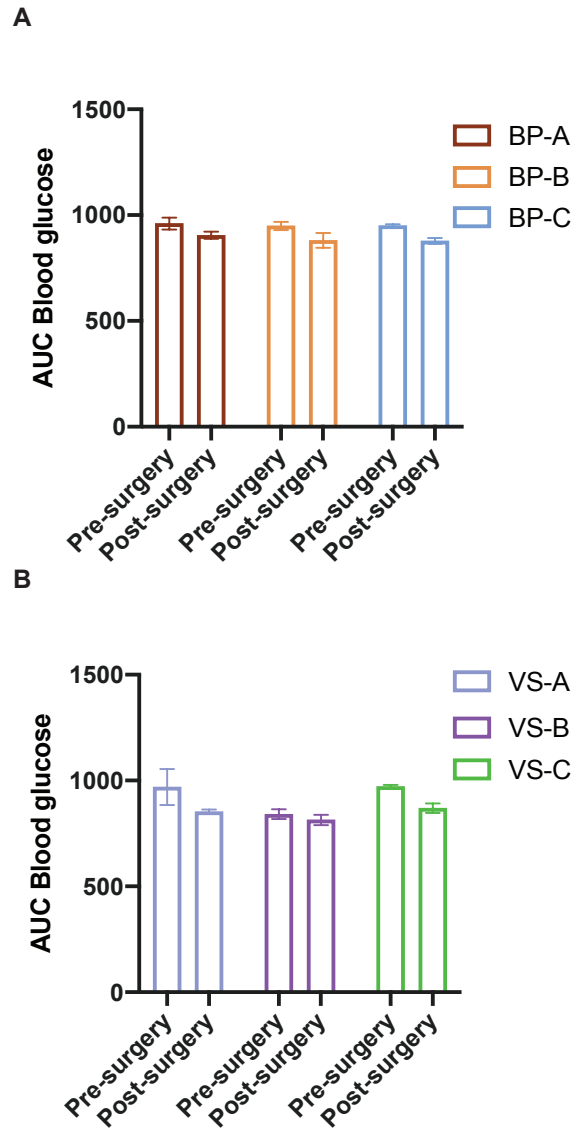


Figure 20: Mice AUC blood glucose at week 7 plotted by donor.

Mice AUC blood glucose at week 7 plotted by donor to examine donor effect. Data was categorized by individual donor underwent BPD/DS (**A**) and VSL (**B**) respectively. Values are mean \pm SEM, n=2 for BP-C Pre-surgery, n=3 for BP-C Post-surgery, VS-A and 3 Pre- and Post-surgery, n=4 for BP-A Pre-surgery, BP-B Post-surgery, VS-B Pre- and Post surgery, n=5 for the remaining groups.

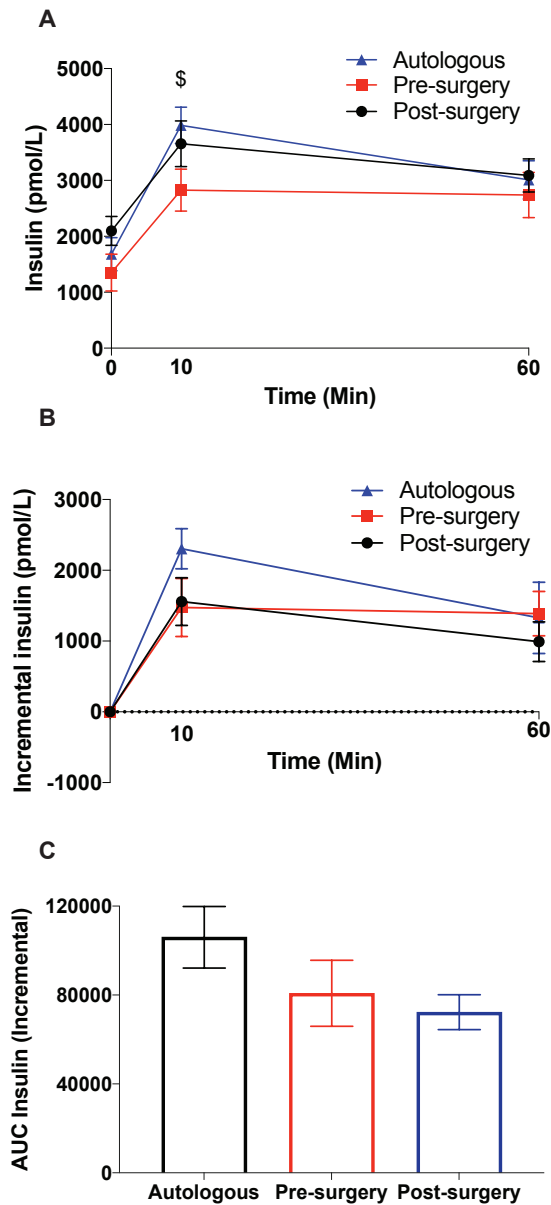


Figure 21: Insulin secretion of female SPF mice received fecal microbiota from BPD/DS donors.

Insulin secretion (**A**), changes in insulin secretion with comparison to base level at t=0 min (**B**) and incremental insulin AUC (**C**) obtained from Multiplex Immunoassay. Values are mean \pm SEM, n=12 for all groups, \$significantly different between autologous and Pre-surgery group.

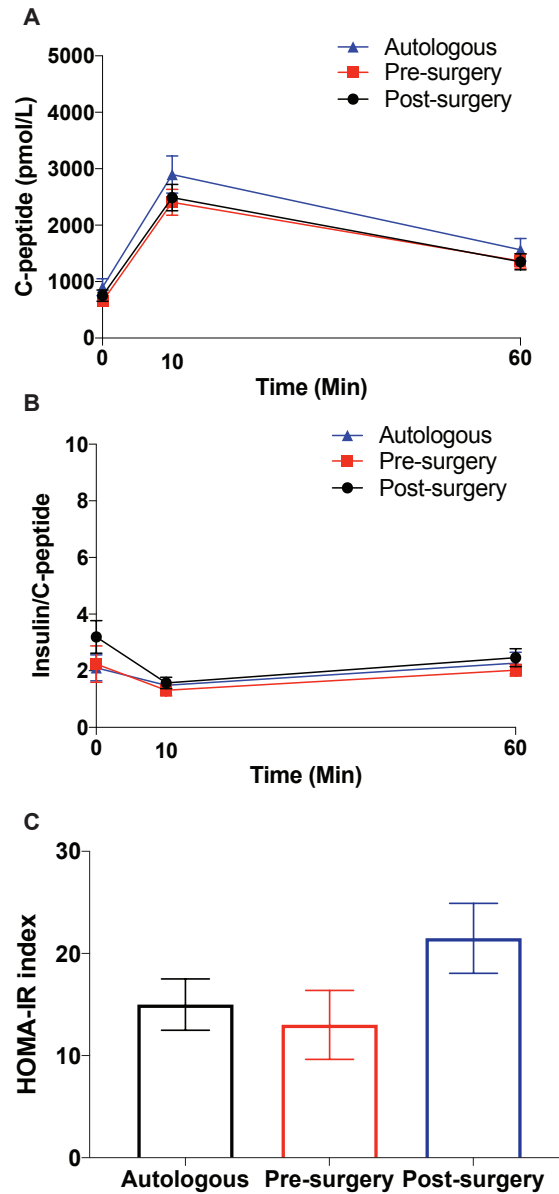


Figure 22: C-peptide secretion, ratio of insulin to c-peptide and HOMA-IR index of female SPF mice received fecal microbiota from BPD/DS donors.

C-peptide secretion (A), ratio of insulin to c-peptide (B) and HOMA-IR index (C) obtained from Multiplex Immunoassay. Values are mean \pm SEM, n=12 for all groups.

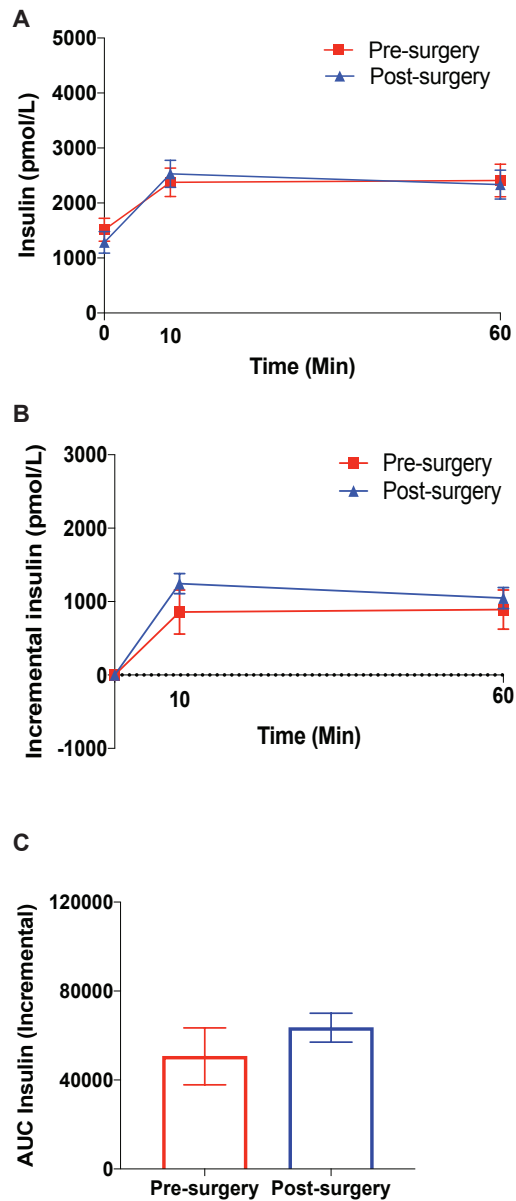


Figure 23: Insulin secretion of female GF mice received fecal microbiota from BPD/DS donors.

Insulin secretion (**A**), changes in insulin secretion with comparison to base level at t=0 min (**B**) and incremental insulin AUC (**C**) obtained from Multiplex Immunoassay. Values are mean \pm SEM, n=11 for Pre-surgery group and n=12 for Post-surgery group.

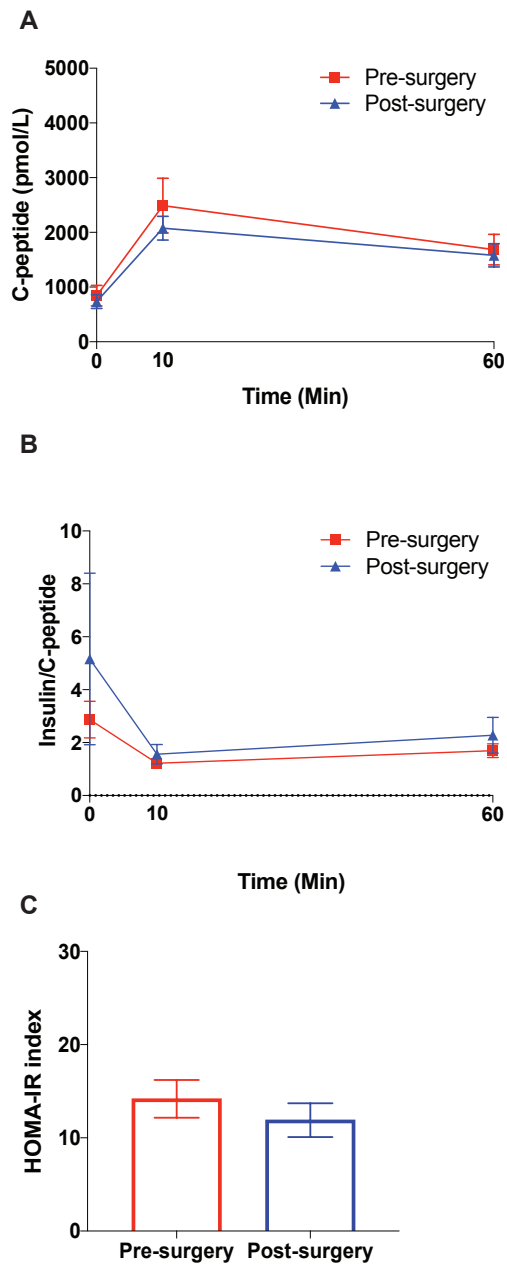


Figure 24: C-peptide secretion, ratio of insulin to c-peptide and HOMA-IR index of female GF mice received fecal microbiota from BPD/DS donors.

C-peptide secretion (A), ratio of insulin to c-peptide (B) and HOMA-IR index (C) obtained from Multiplex Immunoassay. Values are mean \pm SEM, n=11 for Pre-surgery group and n=12 for Post-surgery group.

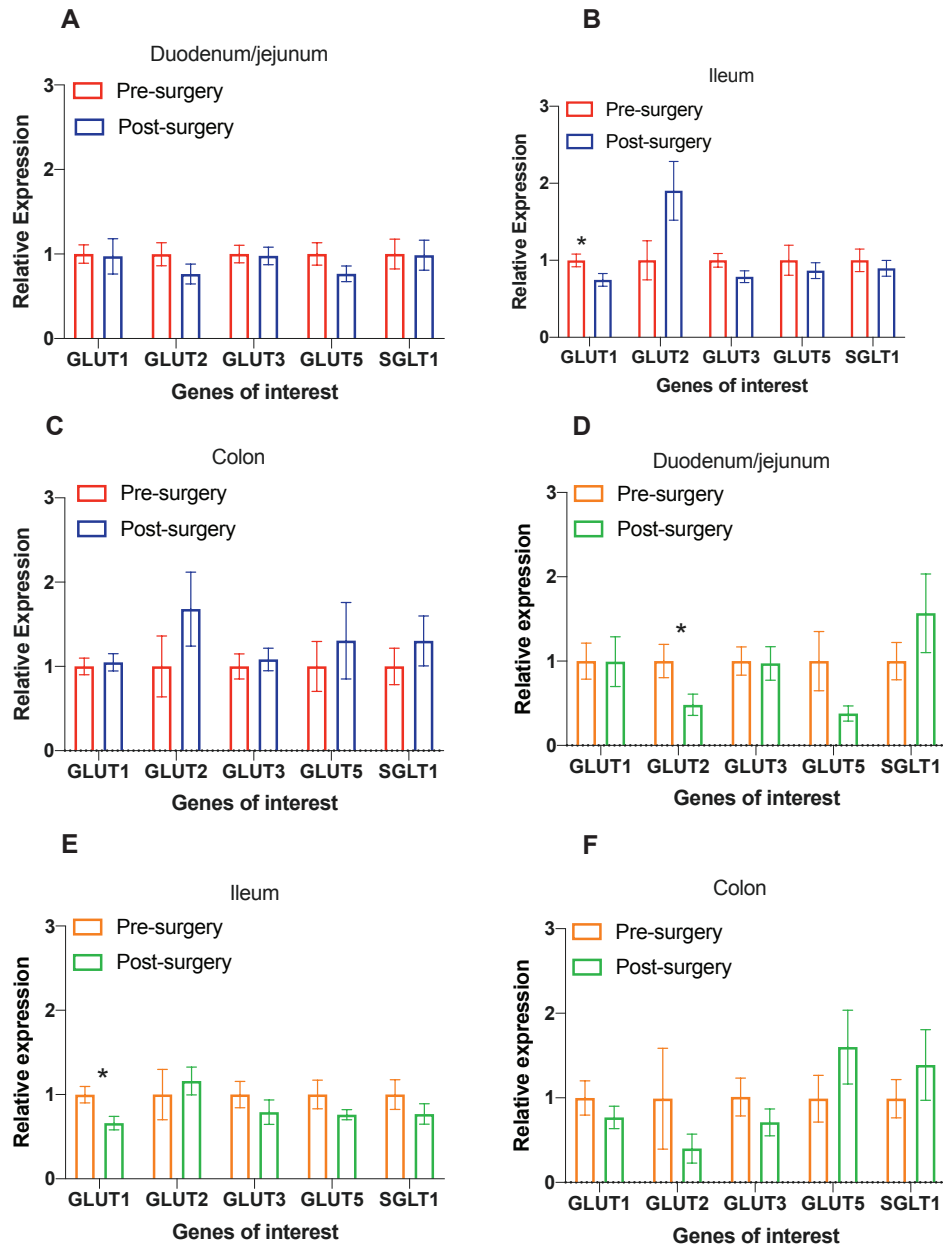


Figure 25: Glucose transporter mRNA expression in female GF mice received fecal microbiota from different bariatric surgery patients.

Glucose transporter mRNA expression in the duodenum/jejunum (A/D), ileum (B/E) and colon (C/F) of female GF mice received fecal microbiota from BPD/DS (A-C) and VSL (D-F) donors respectively. The Pre-surgery group in each graph is used as a reference and have an average value of 1.0. Values are mean \pm SEM, n=9 and n=10 for VSL Pre and Post-surgery group, n=11 and n=12 for BPD/DS Pre and Post-surgery group.

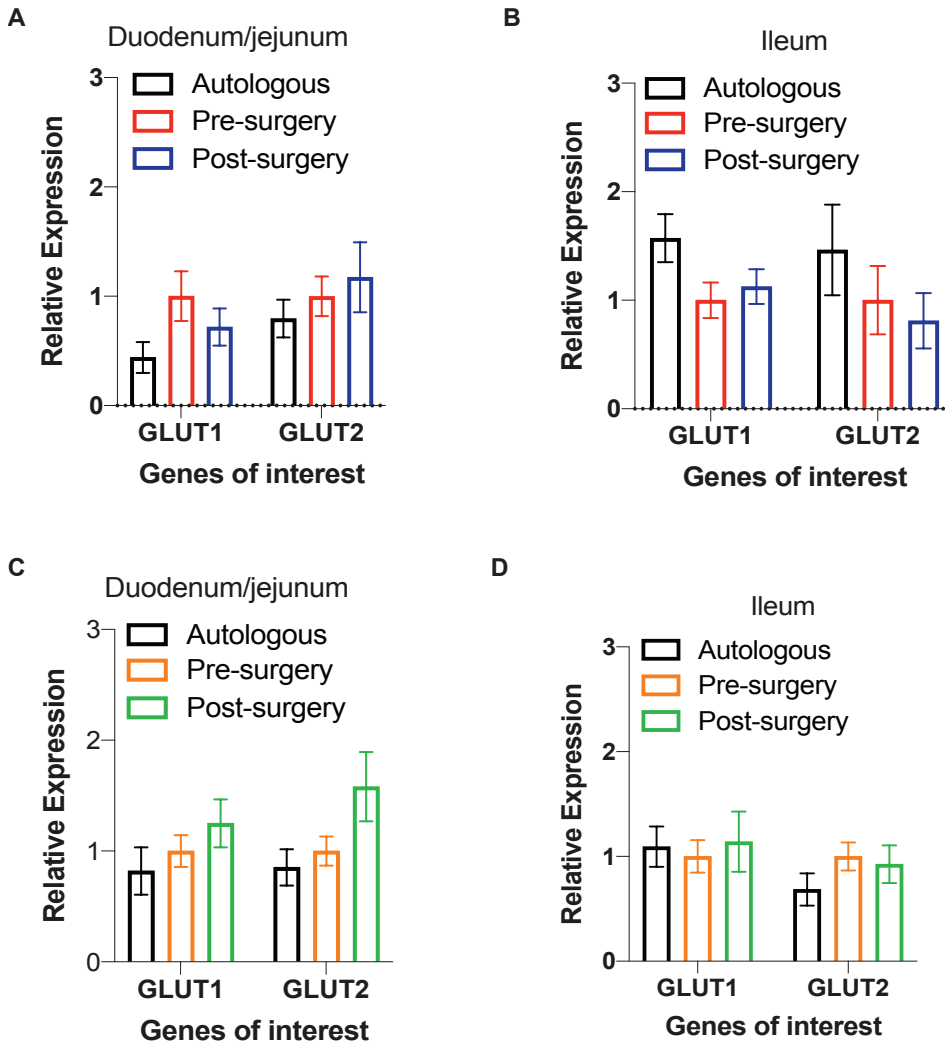


Figure 26: Glucose transporter mRNA expression in female SPF mice received fecal microbiota from different bariatric surgery patients.

Glucose transporter mRNA expression in the duodenum/jejunum (**A/C**) and ileum (**B/D**) of female SPF mice received fecal microbiota from BPD/DS (**A and B**) and VSL (**C and D**) donors respectively. The Pre-surgery group in each graph is used as a reference and have an average value of 1.0. Values are mean \pm SEM, n=12 for all groups.

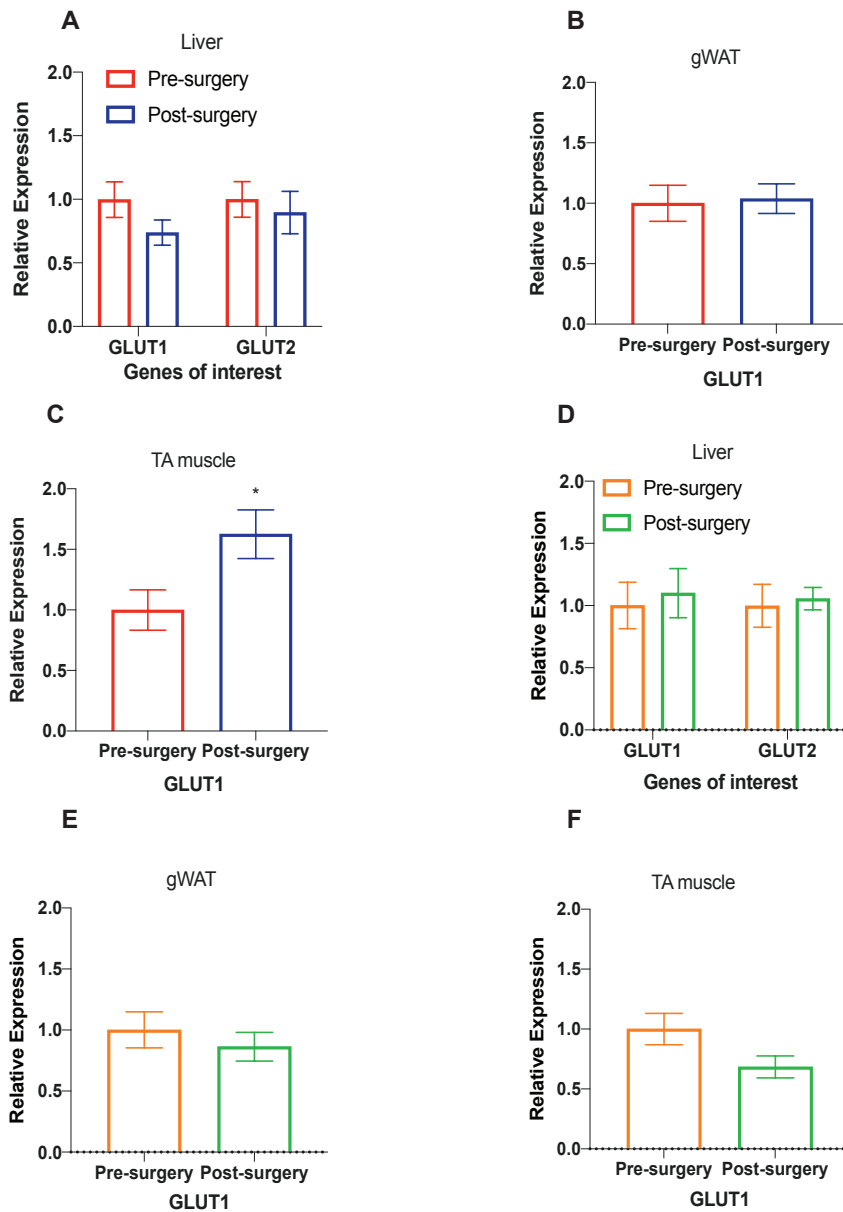


Figure 27: Glucose transporter mRNA expression in female GF mice received fecal microbiota from different bariatric surgery patients.

Glucose transporter mRNA expression in the liver (**A/D**), gWAT (**B/E**) and TA muscle (**C/F**) of female GF mice received fecal microbiota from BPD/DS (**A-C**) and VSL (**D-F**) donors respectively. The Pre-surgery group in each graph is used as a reference and have an average value of 1.0. Values are mean \pm SEM, $n=11$ for BPD/DS Pre and Post-surgery group, $n=10$ for VSL Pre and Post-surgery group. *significantly different from the Pre-surgery group by Mann-Whitney test.

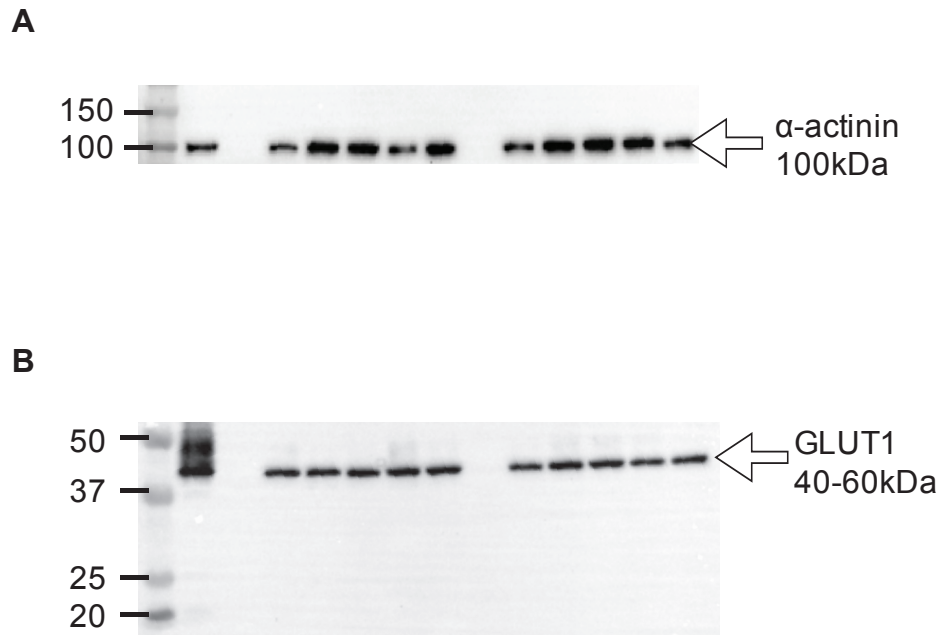


Figure 28: Representative blots.

Example Western blots for α -actinin (**A**) and GLUT1 (**B**). Numbers listed to the left of each image indicates the estimated molecular weights as determined by Bio-rad dual precision ladder (lane 1). For both figures, lane 4-8: samples obtained from GF mice with FMT from pre-surgery VSL patients; lane 10-14: samples obtained from GF mice with FMT from post- surgery VSL patients; lane 2: positive-control with C2C12 cells; lane 3 and 9: blank.

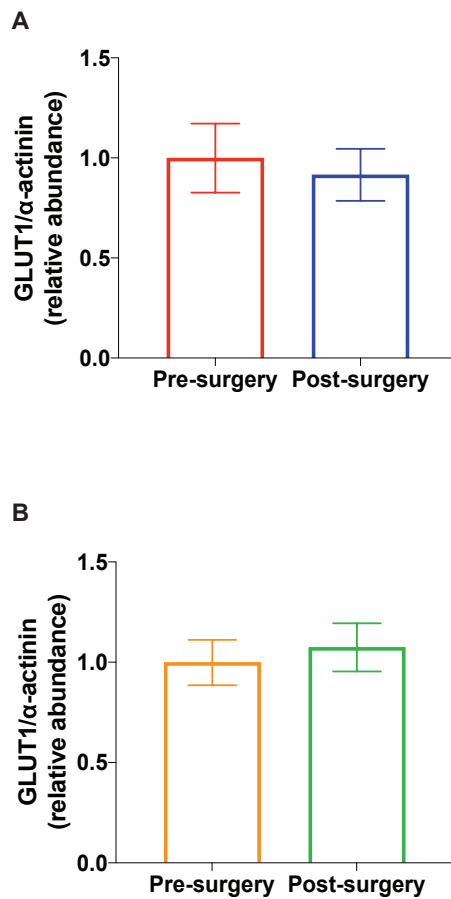


Figure 29: GLUT1/ α -actinin expression in the ileum of female GF mice received fecal microbiota from different bariatric surgery patients.

GLUT1 expression normalized with α -actinin in mice received fecal microbiota from BPD/DS (A) and VSL donors (B). Values are mean \pm SEM, n=10 for VSL Pre and Post-surgery and BPD/DS Pre-surgery group, n=11 for BPD/DS Post-surgery group.

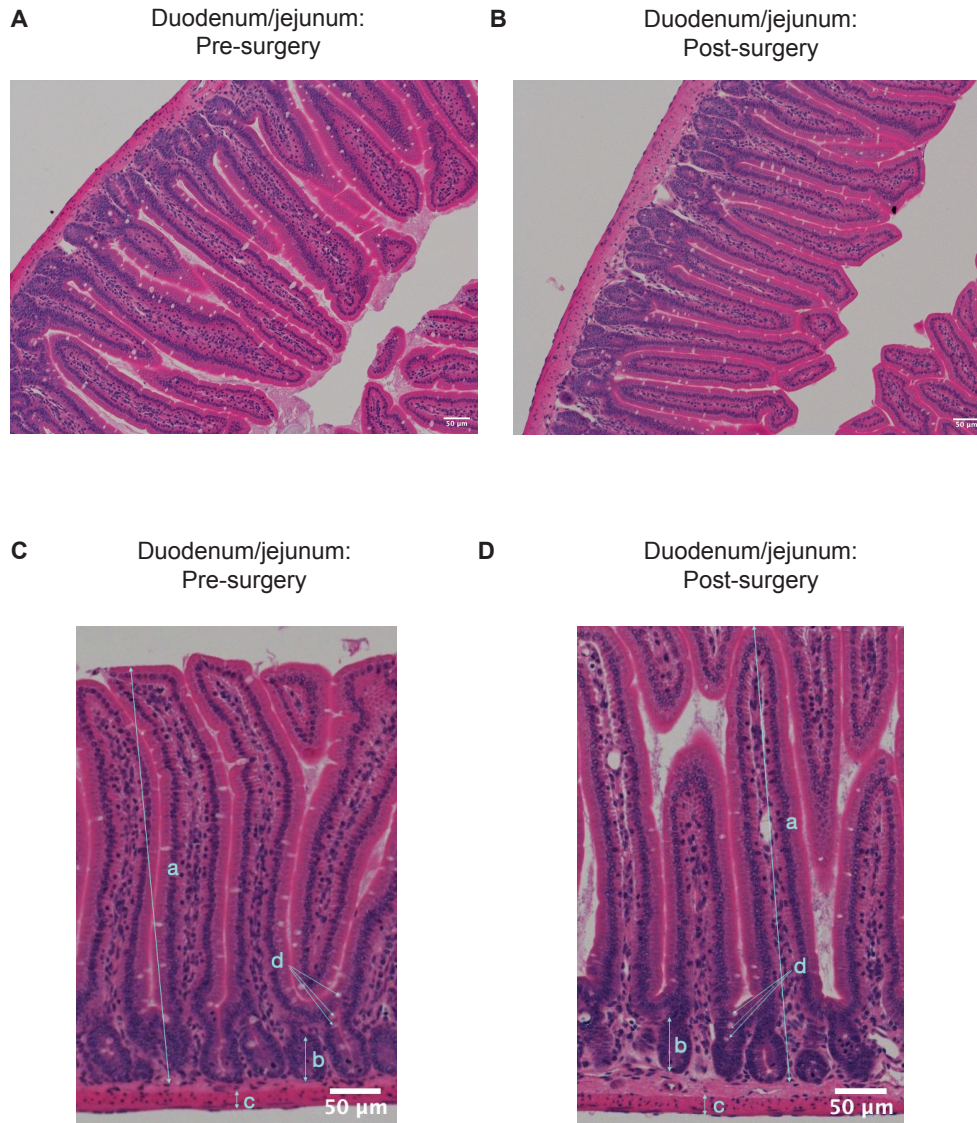


Figure 30: Representative duodenum/jejunum histology images.

Uncropped 10X H&E stained duodenum/jejunum slides from GF mice with BPD/DS donor's Pre- and Post-surgery fecal microbiota (**A and B**). Samples were prepared with Carnoy's solution. One slide was obtained from each sample. Three 10X images and six 20X images were taken from each slide using NIKON Eclipse Ni & Nikon DS-QI2 microscope. The result was analyzed using Image J. Cropped 10X duodenum/jejunum histology images from GF mice with BPD/DS donor's Pre- and Post-surgery fecal microbiota with morphometric characteristics labeling (**C and D**). a: Villus height; b: crypt depth; c: muscular layer thickness; d: goblet cells (clear space).

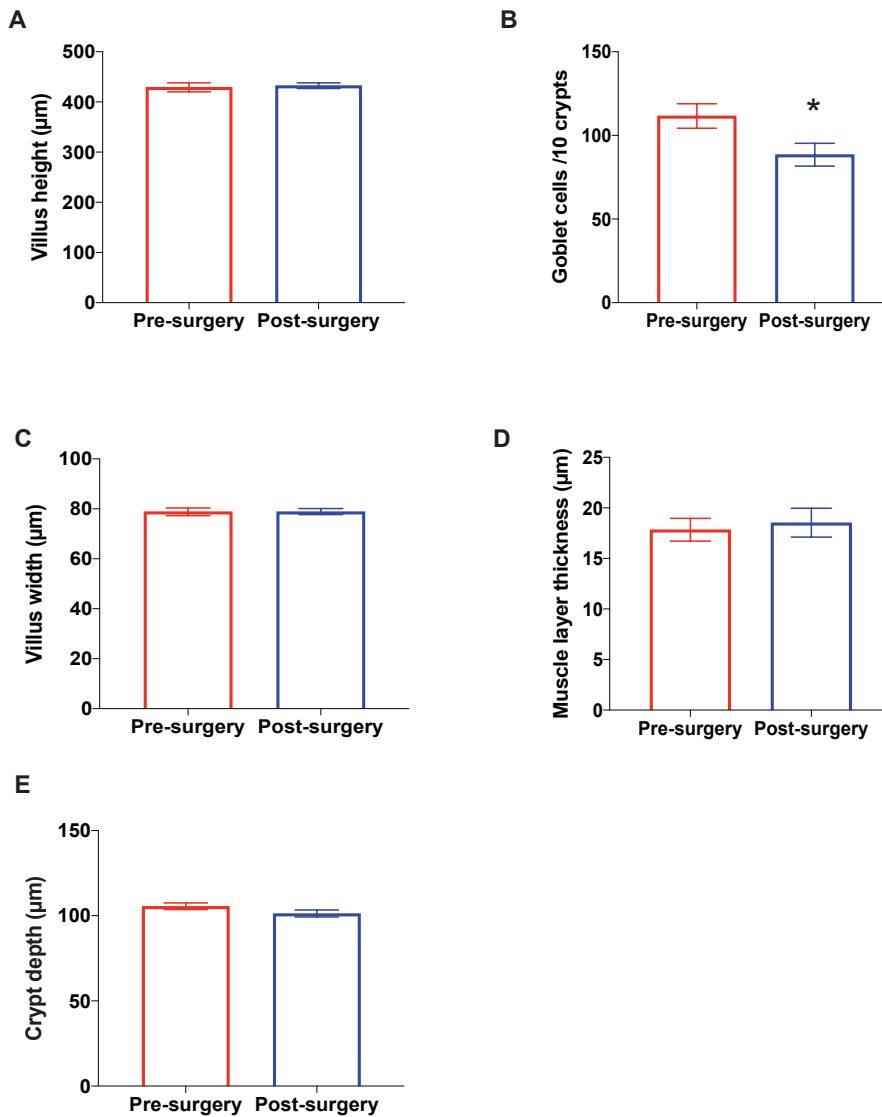


Figure 31: Morphometric characteristics from the duodenum/jejunum segment of mice.

Villus height (A), villus width (C), muscle layer thickness (D) and crypt depth (E) measured from the duodenum/jejunum of GF mice with BPD/DS donor's Pre and Post-surgery fecal microbiota. The number of crypts that contain goblet cells on each image was recorded and used to normalize goblet cell count to per 10 crypts (B). Values are mean \pm SEM, $n > 120$ for both groups in **Figure A**, $n > 24$ for both groups in **Figure B**, $n > 160$ for both groups in **Figure C**, $n = 37$ for both groups in **Figure D** and $n > 275$ for both groups in **Figure E**. *significantly different from the Pre-surgery group by Mann-Whitney test.

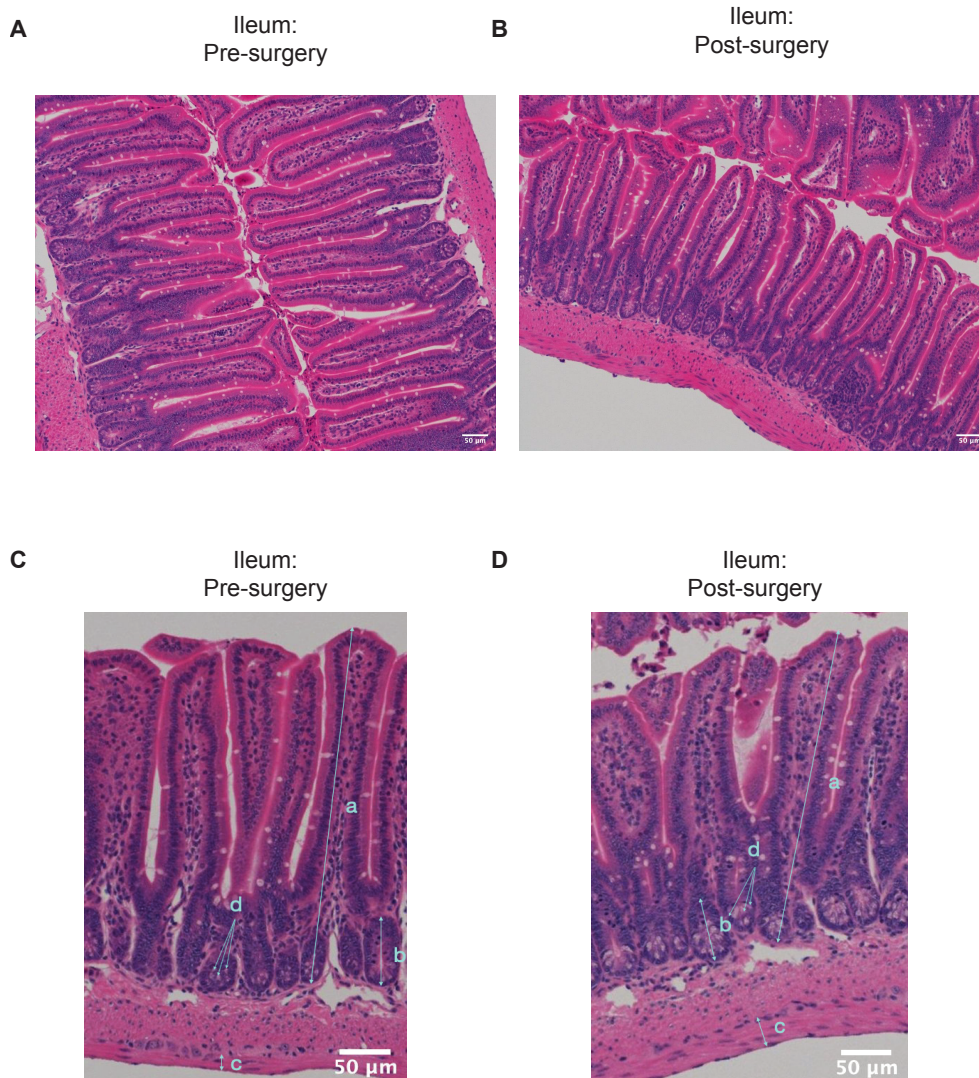


Figure 32: Representative ileum histology images.

Uncropped 10X H&E stained ileum slides from GF mice with BPD/DS donor's Pre- and Post- surgery fecal microbiota (**A and B**). Samples were prepared with Carnoy's solution. One slide was obtained from each sample. Three 10X images and six 20X images were taken from each slide using NIKON Eclipse Ni & Nikon DS-QI2 microscope. The result was analyzed using Image J. Cropped ileum histology images from GF mice with BPD/DS donor's Pre- and Post-surgery fecal microbiota with morphometric characteristics labeling (**C and D**). a: Villus height; b: crypt depth; c: muscular layer thickness; d: goblet cells (clear space).

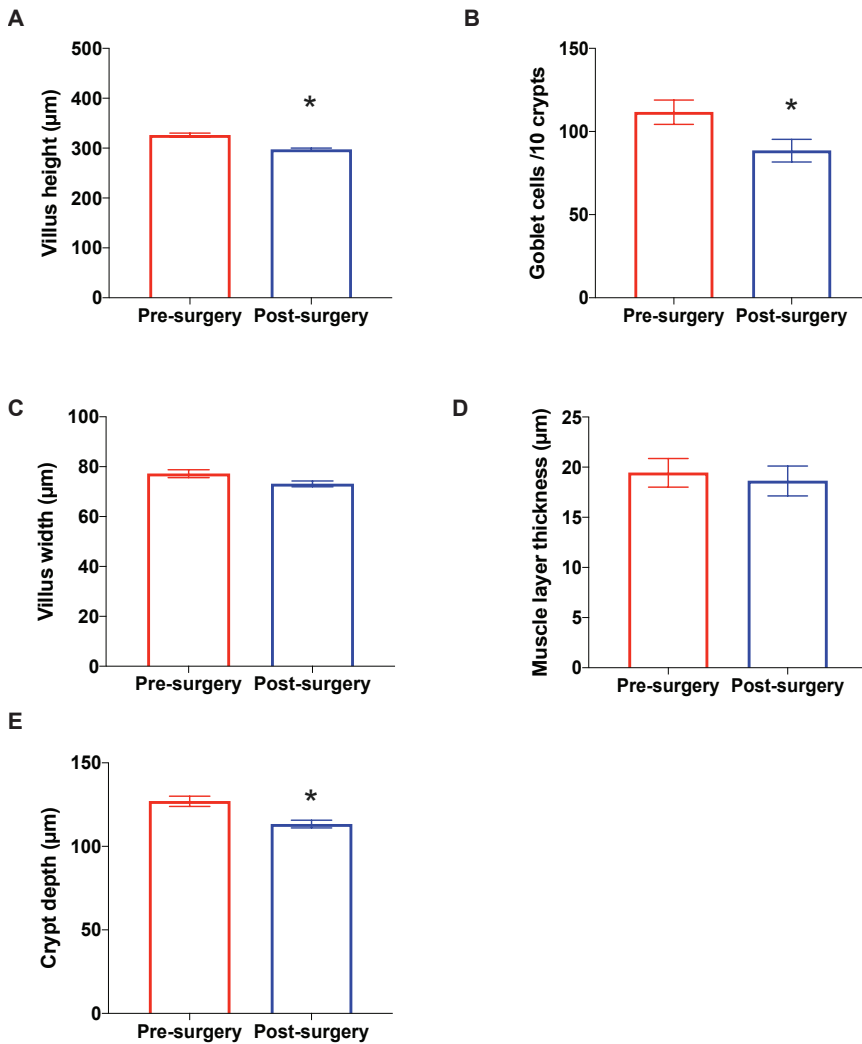


Figure 33: Morphometric characteristics from the ileum segment of mice.

Villus height (A), villus width (C), muscle layer thickness (D) and crypt depth (E) measured from the duodenum/jejunum of GF mice with BPD/DS donor's Pre and Post-surgery fecal microbiota. The number of crypts that contain goblet cells on each image was recorded and used to normalize goblet cell count to per 10 crypts (B). Values are mean \pm SEM, $n > 115$ for both groups in **Figure A**, $n > 24$ for both groups in **Figure B**, $n > 120$ for both groups in **Figure C**, $n > 30$ for both groups in **Figure D** and $n > 210$ for both groups in **Figure E**. *significantly different from the Pre-surgery group by Mann-Whitney test.

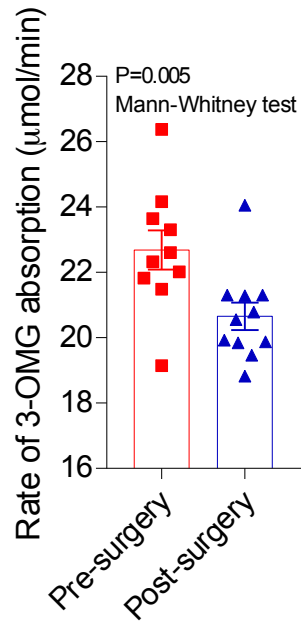


Figure 34: Rate of 3-OMG absorption in female GF mice received fecal microbiota from BPD/DS patients.

Rate of 3-OMG absorption measured at week 7 of the study. Values are mean \pm SEM, n=10 for Pre-surgery group and n=11 for Post-surgery group.